Remote Sensing of Environment 268 (2022) 112764

Contents lists available at ScienceDirect

Remote Sensing of Environment

journal homepage: www.elsevier.com/locate/rse

Large scale multi-layer fuel load characterization in tropical savanna using GEDI spaceborne lidar data

Rodrigo Vieira Leite [a,*], Carlos Alberto Silva [b], Eben North Broadbent [c], Cibele Hummel do Amaral [a], Veraldo Liesenberg [d], Danilo Roberti Alves de Almeida [e], Midhun Mohan [f], Sérgio Godinho [g,h], Adrian Cardil [i,j,k], Caio Hamamura [l], Bruno Lopes de Faria [m], Pedro H.S. Brancalion [e], André Hirsch [n], Gustavo Eduardo Marcatti [n], Ana Paula Dalla Corte [o], Angelica Maria Almeyda Zambrano [p], Máira Beatriz Teixeira da Costa [q], Eraldo Aparecido Trondoli Matricardi [q], Anne Laura da Silva [n], Lucas Ruggeri Ré Y. Goya [n], Ruben Valbuena [r], Bruno Araujo Furtado de Mendonça [s], Celso H.L. Silva Junior [t,u], Luiz E.O. C. Aragão [t,v], Mariano García [w], Jingjing Liang [x], Trina Merrick [y,z], Andrew T. Hudak [aa], Jingfeng Xiao [ab], Steven Hancock [ac], Laura Duncason [ad], Matheus Pinheiro Ferreira [ae], Denis Valle [af], Sassan Saatchi [ag], Carine Klauberg [n]

[a] Department of Forest Engineering, Federal University of Viçosa (UFV), Av. Peter Henry Rolfs, 36570-900 Viçosa, MG, Brazil
[b] Forest Biometrics and Remote Sensing Laboratory (Silva Lab), School of Forest, Fisheries, and Geomatics Sciences, University of Florida, PO Box 110410, Gainesville, FL 32611, USA
[c] Spatial Ecology and Conservation (SPEC) Lab, School of Forest, Fisheries, and Geomatics Sciences, University of Florida, Gainesville, FL 32611, USA
[d] Department of Forest Engineering, College of Agriculture and Veterinary, Santa Catarina State University (UDESC), Lages, SC, Brazil
[e] Department of Forest Sciences, "Luiz de Queiroz" College of Agriculture, University of São Paulo (USP/ESALQ), Piracicaba, SP, Brazil
[f] Department of Geography, University of California—Berkeley, Berkeley, CA 94709, USA
[g] EaRSLab—Earth Remote Sensing Laboratory, University of Évora, 7000-671 Évora, Portugal
[h] Institute of Earth Sciences (ICT), Universidade de Évora, Rua Romão Ramalho, 59, 7002-554 Évora, Portugal
[i] Technosylva Inc, La Jolla, CA, USA
[j] Department of Crop and Forest Sciences, University of Lleida, Lleida, Spain
[k] Joint Research Unit CTFC - AGROTECNIO, Solsona, Spain
[l] Federal Institute of Education, Science and Technology of São Paulo, SP 11533-160, Brazil
[m] Department of Forest Science, Federal University of Vales do Jequitinhonha e Mucuri (UFVJM), Campus JK, Diamantina, MG, Brazil
[n] Federal University of São João Del Rei – UFSJ, Sete Lagoas, MG 35701-970, Brazil
[o] Department of Forest Engineering, Federal University of Paraná (UFPR), Curitiba 80.210-130, PR, Brazil
[p] Spatial Ecology and Conservation (SPEC) Lab, Center for Latin American Studies, University of Florida, Gainesville, FL 32611, USA
[q] Department of Forestry, University of Brasília, Campus Darcy Ribeiro, Brasilia, DF 70.910-900, Brazil
[r] School of Natural Sciences, Bangor University, Bangor LL57 2W, UK
[s] Silviculture Department, Universidade Federal Rural do Rio de Janeiro, Rua da Floresta, Seropédica, RJ 23897-005, Brazil
[t] National Institute for Space Research, Earth Observation and Geoinformatics Division, Av. dos Astronautas, 1758, São José dos Campos, SP 12227-010, Brazil
[u] Universidade Estadual do Maranhão (UEMA), Departamento de Engenharia Agrícola, São Luís, MA 65055-310, Brazil
[v] College of Life and Environmental Sciences, University of Exeter, Exeter, UK
[w] Environmental Remote Sensing Research Group, Department of Geology, Geography and the Environment, Universidad de Alcalá, Calle Colegios 2, Alcalá de Henares 28801, Spain
[x] Department of Forestry and Natural Resources, Purdue University, West Lafayette, IN, USA
[y] Department of Earth and Environmental Science, Vanderbilt University, Nashville, TN 37240, USA
[z] Department of Geography, Florida State University, Tallahassee, FL, USA
[aa] US Department of Agriculture, Forest Service, Rocky Mountain Research Station, 1221 South Main Street, Moscow, ID 83843, USA
[ab] Earth Systems Research Center, Institute for the Study of Earth, Oceans, and Space, University of New Hampshire, Durham, NH 03820, USA
[ac] School of GeoSciences, University of Edinburgh, UK
[ad] Department of Geographical Sciences, University of Maryland, College Park, MD 20740, USA
[ae] Cartographic Engineering Section, Military Institute of Engineering (IME), Praça Gen. Tibúrcio 80, 22290-270 Rio de Janeiro, RJ, Brazil
[af] School of Forest, Fisheries, and Geomatics Sciences, University of Florida, PO Box 110410, 136 Newins-Ziegler Hall, Gainesville, FL 32611, USA
[ag] NASA-Jet Propulsion Laboratory, California Institute of Technology, Pasadena, CA 91109, USA

* Corresponding author.
E-mail addresses: rodrigo.leite@ufv.br (R.V. Leite), c.silva@ufl.edu (C.A. Silva), carine_klauberg@hotmail.com (C. Klauberg).

https://doi.org/10.1016/j.rse.2021.112764

Available online 30 October 2021

ARTICLE INFO

Editor: Marie Weiss

Keywords:
Active remote sensing
Fire
Modeling
Machine learning
UAV-lidar
Cerrado
Vegetation structure

ABSTRACT

Quantifying fuel load over large areas is essential to support integrated fire management initiatives in fire-prone regions to preserve carbon stock, biodiversity and ecosystem functioning. It also allows a better understanding of global climate regulation as a potential carbon sink or source. Large area assessments usually require data from spaceborne remote sensors, but most of them cannot measure the vertical variability of vegetation structure, which is required for accurately measuring fuel loads and defining management interventions. The recently launched NASA's Global Ecosystem Dynamics Investigation (GEDI) full-waveform lidar sensor holds potential to meet this demand. However, its capability for estimating fuel load has yet not been evaluated. In this study, we developed a novel framework and tested machine learning models for predicting multi-layer fuel load in the Brazilian tropical savanna (i.e., Cerrado biome) using GEDI data. First, lidar data were collected using an unnamed aerial vehicle (UAV). The flights were conducted over selected sample plots in distinct Cerrado vegetation formations (i.e., grassland, savanna, forest) where field measurements were conducted to determine the load of surface, herbaceous, shrubs and small trees, woody fuels and the total fuel load. Subsequently, GEDI-like full-waveforms were simulated from the high-density UAV-lidar 3-D point clouds from which vegetation structure metrics were calculated and correlated to field-derived fuel load components using Random Forest models. From these models, we generate fuel load maps for the entire Cerrado using all on-orbit available GEDI data. Overall, the models had better performance for woody fuels and total fuel loads ($R^2 = 0.88$ and 0.71, respectively). For components at the lower stratum, models had moderate to low performance (R^2 between 0.15 and 0.46) but still showed reliable results. The presented framework can be extended to other fire-prone regions where accurate measurements of fuel components are needed. We hope this study will contribute to the expansion of spaceborne lidar applications for integrated fire management activities and supporting carbon monitoring initiatives in tropical savannas worldwide.

1. Introduction

Climate change mitigation and biodiversity conservation efforts across the world require an understanding of wildfire dynamics (Bowman et al., 2013; Lehmann et al., 2014). Tropical Savanna ecosystems are generally fire-adapted (Simon et al., 2009; Hoffmann et al., 2012; Durigan and Ratter, 2016), but human activities have affected fire regimes and landscape characteristics (Hantson et al., 2015; Andela et al., 2017; Andela et al., 2018; Rosan et al., 2019; Durigan et al., 2020). Fire dynamics in tropical savannas depend, among other factors, on the vegetation structure and accumulated fuel loads (combustible contents) (Sandberg et al., 2001; Chuvieco et al., 2003; Keane et al., 2013). Fuel load structure continuity, condition (live or dead) and moisture are important variables for modeling fire behavior (Stavros et al., 2018; Gomes et al., 2020a), assessing its severity (Hu et al., 2019; Klauberg et al., 2019), calculating greenhouse gas emissions (GHG) (Ogle et al., 2019; Gomes et al., 2020a) and improving landscape management and conservation strategies to promote a pyro-diverse ecosystem (Schmidt et al., 2018; Franke et al., 2018). These applications demand measurements of all fuel components as they interact with fire differently. That includes necromass (e.g., duff, litter, downed wood debris) and different plant types (e.g., grasses, herbs, forbs, shrubs, trees).

Remote sensing technologies are commonly used to examine fuel load distribution and spatial variability over large areas. In this regard, lidar (light detection and ranging) sensors are preferred as they can directly detect different vegetation strata with high accuracy (Erdody and Moskal, 2010, Gajardo et al., 2014, Szpakowski and Jensen, 2019, Chuvieco et al., 2020). Generally, the approach for local scale fuel mapping relies on discrete-return or full-waveform lidar sensors in aircraft or unnamed aerial vehicle (UAV) platforms to collect lidar data and calculate lidar-derived metrics that will subsequently serve as predictor variables in statistical models (Hermosilla et al., 2014; Hudak et al., 2016a; Bright et al., 2017; Stefanidou et al., 2020). Nonetheless, when there are limited resources for airborne and UAV-lidar surveys, or it is necessary to upscale analyses to a regional/global level, images acquired by satellite systems operating in either optical or microwave domain are then required (Wulder et al., 2012; García et al., 2017; Franke et al., 2018). The Geoscience Laser Altimeter System (GLAS, onboard ICESat-1 – Zwally et al., 2002) was the first spaceborne lidar sensor to collect sample data globally, and it was operational between 2003 and 2009. Although its main objective was to measure ice-sheet changes, GLAS was also used for forest and fuel-related studies (Lefsky et al., 2006; Duncanson et al., 2010; Ashworth et al., 2010; García et al., 2012; Peterson et al., 2013; Ferreira et al., 2011). Its successor mission launched in 2018, ICESat-2, is a photon-counting lidar system that also provides valuable 3-D sample data globally that can be similarly used for biomass estimation (Narine et al., 2020). Yet, neither of these missions' characteristics were optimized for collecting data over the global range of forest canopy structures which limits opportunities to use these data to examine some important biomes at regional scale.

A new promising near-global dataset for fuel load estimation comes from the Global Ecosystem Dynamics Investigation (GEDI) sensor, with unprecedented high resolution lidar data samples collected between ~52° north and south latitudes, available since April 2019 (Dubayah et al., 2020). As the first of its kind, GEDI was specifically designed to measure forest structure. The sensor is characterized as a large-footprint (diameter of ~25 m) full-waveform lidar with penetration capability in forests with up to ~99% canopy cover (Hancock et al., 2019; Duncanson et al., 2020). GEDI's penetration capabilities in dense vegetation is what mainly differentiates it from the previous spaceborne lidar sensors designed for ice sheet measurements. Furthermore, the footprints are separated at 60 m along track and 600 m across track - an improvement to GLAS' 70 m footprint separated ~170 m along track (Zwally et al., 2002). The improved technical specification makes GEDI more suitable than any previous spaceborne sensor to measure forest structure at regional and global scales.

The GEDI mission plan includes the delivery of a global aboveground dry biomass (AGB) product at a spatial resolution of 1-km (Dubayah et al., 2020) that is suitable for global biomass mapping requirements (Hall et al., 2011). These AGB estimates are expected to be the global benchmark of forest AGB, essential for measuring the world's carbon stocks. Furthermore, recent studies used GEDI waveform metrics for developing models to estimate forest height (Potapov et al., 2021; Rishmawi et al., 2021), biomass (Saarela et al., 2018; Silva et al., 2021; Duncanson et al., 2020; Rishmawi et al., 2021), and canopy structure diversity (Marselis et al., 2018; Schneider et al., 2020; Rishmawi et al., 2021). However, to date, no published study on estimation of fuel loads from GEDI data is available and the GEDI AGB products may be of limited use for fire-related applications because calibration data to derive information on important layers may be lacking – such as from

duff, litter, down woody debris, grasses, forbs and shrubs. In addition, these lower fuel strata layers that are crucial for fire behavior and emissions are commonly not considered in previous studies using spaceborne lidar sensors (Lefsky et al., 2005; García et al., 2012; Peterson et al., 2013). Therefore, it is necessary to develop models using GEDI-derived metrics that consider all fuel load components for effectively meeting integrated fire management criteria and for improving carbon budget estimates.

Confirming GEDI's capability to predict fuel loads in savannas will open a range of new opportunities to improve fire management planning and decisions at regional and global scales. Furthermore, the possibility of having this information from space also opens the range of GEDI applications to map fuel loads during the mission life-span and for upcoming lidar satellite missions (e.g., Multi-footprint Observation Lidar and Imager - MOLI (Murooka et al., 2013, Kimura et al., 2017, Asai et al., 2018). The applications of such technological advances include mapping fire risk, carbon emissions and estimate fire behavior and fuel load dynamics for larger areas such as countries or entire biomes, thus contributing to mitigate the impacts of climate change in these regions. The overall aim of this study was to assess the capability of GEDI for estimating large-scale multi-layer fuel loads in the Brazilian tropical savanna (Cerrado). Herein, we developed a framework to i) calibrate and validate Random Forest (RF) models for predicting different fuel layers (ground, surface, shrubs, trees and total fuel load) at the plot level across the complex gradient of Cerrado formations (i.e., grassland, savanna and forest) in Brazil from field and simulated GEDI data; and ii) characterize large-scale, multi-layer fuel loads across the entire Cerrado (i.e. 1.9 million km^2) by applying the calibrated RF models to on-orbit GEDI data collected over its whole extent, and then aggregating the footprint level fuel load estimates to 1-km-resolution grid across the biome.

2. Material and methods

2.1. Study area

Cerrado is the most biodiverse savanna in the world and considered as a top global hotspot for conservation priorities (Myers et al., 2000). It has been rapidly converted to crop and pasturelands and less than half of its original vegetation cover remains (Strassburg et al., 2017). This native vegetation, however, has been severely impacted by human-mediated shifts in fire regimes and widespread invasion of fire-prone African fodder grasses (Durigan and Ratter, 2016). Our study sites are located in the Serra do Cipó National Park (SCNPK), Chapada dos Veadeiros National Park (CVNPK), Paraopebas National Forest (PNF) and University of São João Del-Reis Forest (UFSJ) (Fig. 1). Site locations were chosen to span a range of vegetation structures within the Cerrado biome, covering the three major formations (i.e., grassland, savanna, and forest). In Cerrado, grasslands are characterized by the presence of grass species alone (vegetation type locally known as "Campo limpo"), with scattered shrubs ("Campo sujo" and "Campo rupestre"), or dominated by grasses and shrubs with scattered trees ("Cerrado ralo"). The savanna formation is mostly dominated by contorted short trees with scattered shrubs and grasses (e.g., "Cerrado sensu stricto"). Forests are

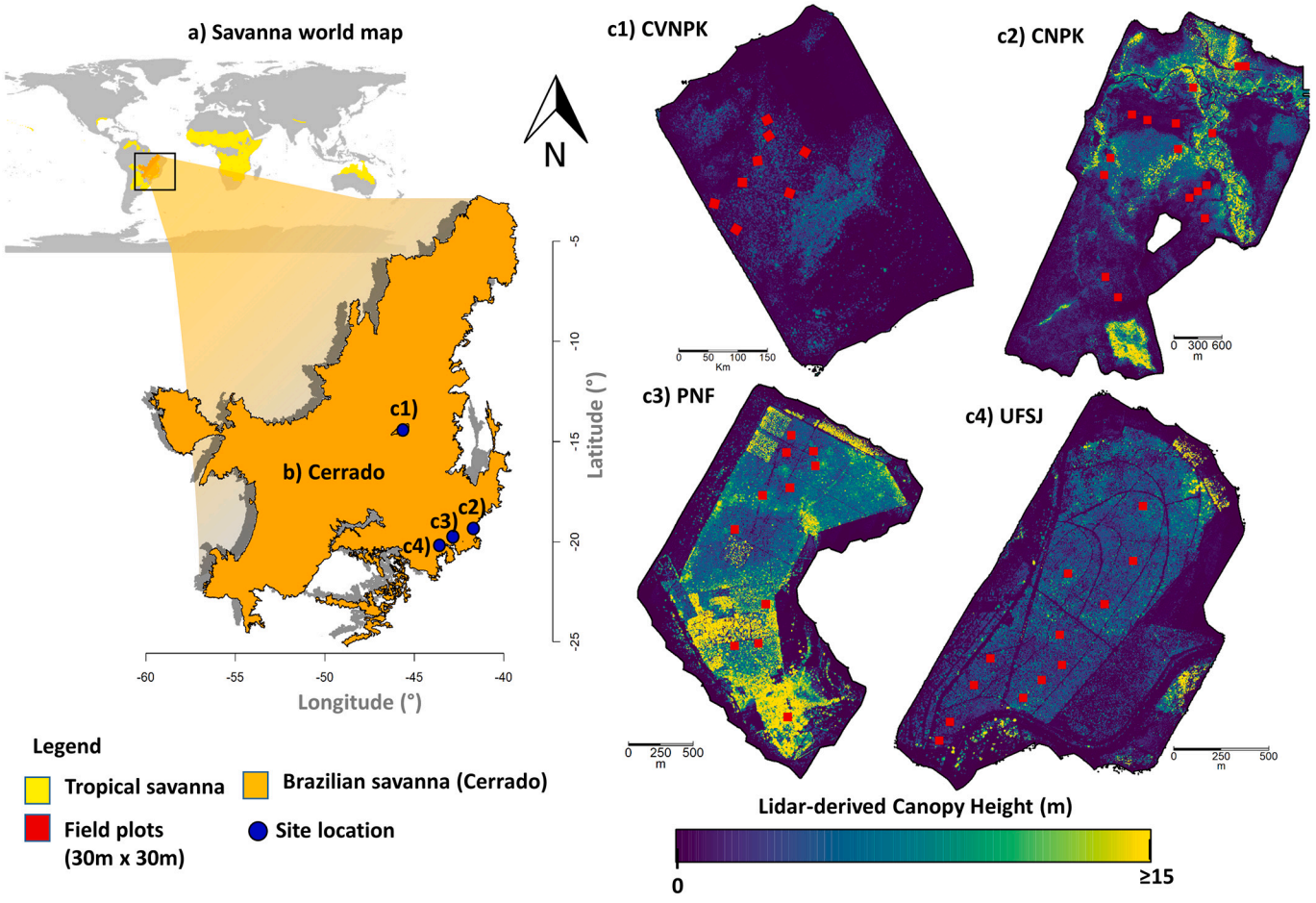

Fig. 1. Spatial location of the Brazilian savanna (Cerrado) (a, b) and study sites where UAV-lidar and field data were collected, namely, Chapada dos Veadeiros National Park (CVNPK, c1), Serra do Cipó National Park (SCNPK, c2) Paraopeba National Forest (PNF, c3) and University of São João Del-Rei's Forest (UFSJ, c4). Fig. c1-c4 show the UAV-lidar coverage and canopy height model derived from the 3D point cloud.

tree-dominated formations (e.g., "Cerradão", in addition to the extra-Cerrado forest formations as Riparian and Gallery forests). For further study site characteristics regarding their location, seasonal/climate traits, soil characteristics and topography, please refer to section 2.1 in da Costa et al. (2021).

2.2. Fuel load measurements

We established sample plots in different Cerrado vegetation formations (i.e., grassland, savanna, and forest) between June and July 2019. First, 50 square plots of 30 × 30 m (900 m^2) were set across the study sites (Fig. 2a). Each plot corner was geolocated using a Differential Global Navigation Satellite System (Fig. 2c). Subsequently, four 1 × 1 m (1 m^2) and two 1 × 5 m (5 m^2) subplots were set within each plot to measure surface and shrubs/small trees fuel components, respectively (Fig. 2b, d). In the field, all duff, litter and downed woody debris (surface fuels; SU_{fuels}) were separated from non-woody grasses, herbs and forbs (herbaceous fuels; HB_{fuels}). They were immediately weighed with a 10 g precision scale. Three 500 g samples were taken to be weighed on a laboratory scale (precision of 1 mg) and oven dried at 65 °C until a constant weight was reached. The fresh and dry weight of the samples were used to calculate fuel moisture content (FMC, Eq. (1)). The total dry biomass of SU_{fuels} and HB_{fuels} were then calculated for the plots using Eqs. (2) and (3). In addition, SU_{fuels} and HB_{fuels} were summed up to create a single component of the lowest stratum SH_{fuels} (Eq. (4)).

$$FMC(\%) = (FW - DW)/DW \tag{1}$$

where: FW is the sample's fresh weight (g) measured in the field and DW is its oven-dried weight (g).

$$SU_{fuels} = \sum_{i=1}^{n}((duff_i(kg) + litter_i(kg) + downed\ wood_i(kg)) \; x\ (1 - FMC))\ x\ HEF_{SU} \tag{2}$$

where: SU_{fuels} is the total dry biomass (Mg ha^{-1}) of duff, litter and downed wood collected in sub-plot i. HEF_{SU} is the hectare expansion factor of 2.5 used to convert from kg to Mg ha^{-1}.

$$HB_{fuels} = \sum_{i=1}^{n}((non - woody\ grasses_i\ (kg) + forbs_i(kg))\ x\ (1 - FMC))\ x\ HEF_{SU} \tag{3}$$

where: HB_{fuels} is the total dry biomass (Mg ha^{-1}) in plot i of non-woody grasses and forbs collected in subplot j.

$$SH_{fuels} = SU_{fuels} + HB_{fuels} \tag{4}$$

where: SH_{fuels} is the total dry biomass (Mg ha^{-1}) of the lowest vegetation stratum.

Similarly, all the shrubs and trees with diameter at breast height (dbh, 1.3 m) < 10 cm were harvested and immediately weighed with a 10 g precision scale. Three 500 g samples of stems, branches and leaves were taken to be weighed in a laboratory scale (precision 1 mg) and oven dried at 65 °C until constant weight was reached. The total dry biomass of this component was then calculated using Eq. (5).

$$SS_{fuels} = \sum_{i=1}^{n}((shrubs_i\ (kg) + small\ trees_i\ (kg))\ x\ (1 - FMC))\ x\ HEF_{SS} \tag{5}$$

where: SS_{fuels} is the total dry biomass (Mg ha^{-1}) of shrubs and small trees (dbh < 10 cm). HEFss = 2.5.

Finally, all the trees in the plots with $dbh \geq 10$ cm were measured for total height (ht) and dbh using a digital clinometer and diameter tape, respectively. We used those measurements to estimate the dry aboveground biomass of trees (WD_{fuels}) using Eq. (6) (Chave et al., 2014).

$$WD_{fuels} = \sum_{j=1}^{n} 0.0673\ x\ (\rho\ x\ dbh_j^2\ x\ ht_j)^{0.976}\ x\ HEF_{wd} \tag{6}$$

where: WD_{fuels} is the total dry aboveground biomass of trees (Mg ha^{-1}); dbh_j and ht_j are the dbh (cm) and ht (m) per tree j; ρ is the wood density (g cm^{-3}) derived from Zanne et al. (2009). HEFwd = 0.011. The total fuel load (TF_{fuels}) was calculated by summing all the components (Eq. (7)). Table 1 summarizes fuel load component values in the sample plots

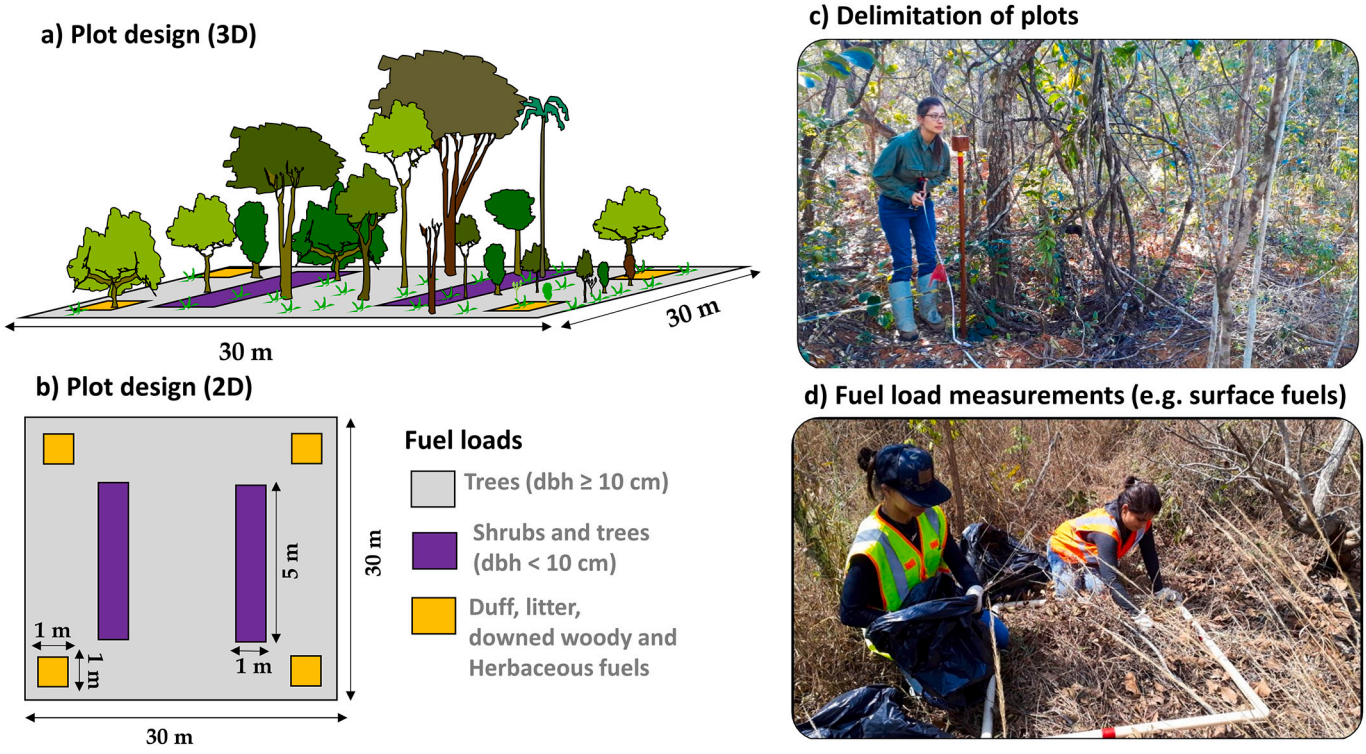

Fig. 2. Summary of field data survey where different plot sizes were designed for collecting tree, shrub, and surface fuels (a, b). Subfigures c) and d) depict plot sampling configuration and surface fuel collection, respectively.

Table 1
Summary of field measurements of surface fuels (SU_{fuels}), herbaceous (HB_{fuels}), surface and herbaceous fuels (SH_{fuels}), shrubs (SS_{fuels}, dbh < 10 cm), woody fuels (WD_{fuels}, dbh ≥ 10 cm) and total fuel load (TF_{fuels}) over the different Cerrado formations (i.e., grassland, savanna and forests).

Cerrado formation	Number of plots	Fuel component	Fuel load (Mg ha^{-1})			
			min	max	mean	sd
Grassland	5	SU_{fuels}	2.7	10.3	5.1	3.1
		HB_{fuels}	3.7	19.9	10.6	6.8
		SH_{fuels}	6.6	25.6	15.7	8.5
		SS_{fuels}	0.1	4.5	1.4	1.8
		WD_{fuels}	0.0	0.6	0.1	0.3
		TF_{fuels}	11.7	25.9	17.2	7.3
Savanna	30	SU_{fuels}	2.0	22.4	8.0	4.1
		HB_{fuels}	0.6	7.7	3.7	1.9
		SH_{fuels}	3.8	26.1	11.7	4.5
		SS_{fuels}	0.5	39.7	10.1	9.2
		WD_{fuels}	0.0	55.6	18.6	17.1
		TF_{fuels}	13.3	100.2	40.4	23.5
Forest	15	SU_{fuels}	0.8	30.1	13.9	7.3
		HB_{fuels}	0.4	6.7	1.3	1.6
		SH_{fuels}	1.3	30.7	15.3	7.8
		SS_{fuels}	0.0	36.8	11.9	13.1
		WD_{fuels}	25.9	138.1	77.1	39.2
		TF_{fuels}	43.7	187.9	104.2	42.4

by each Cerrado formation and a description of the data collection authorization process is in the supplementary material.

$$TF_{fuels} = SU_{fuels} + HB_{fuels} + SS_{fuels} + WD_{fuels} \quad (7)$$

2.3. UAV-lidar data acquisition and processing

The UAV-lidar 3-D point clouds were acquired with the GatorEye Gen 1 UAV system (Broadbent et al., 2021) in July 2019. The GatorEye platform was a DJI M600 Pro hexacopter that integrated a Velodyne VLP-32c dual-return laser scanner lidar with an Inertial Measurement Unit (Fig. 3), and it was coupled with a dual-return lidar sensor with 32 separate lasers, each having a 360° vertical field of view (FOV). The sensor emitted around 600,000 pulses per second with a theoretical return number of 1.2 million returns per second and in parallel, a Global Navigation Satellite System (GNSS) receiver collected static geolocation data to calculate a post-processing kinematic (PPK) flight trajectory. Herein, UAV-lidar 3D point cloud data processing included implementing the GatorEye Multi-scalar Post-Processing Workflow (as detailed in Broadbent et al., 2021), aligning the flight lines, and clipping the point clouds within the field plots for GEDI data simulation (Section 2.4).

2.4. GEDI data

2.4.1. GEDI full-waveform simulation

We simulated GEDI data from the UAV-lidar 3D point cloud for calibrating fuel load models to avoid the geolocation errors of GEDI (~10–20 m) and due to the fact that GEDI orbits are likely not to overlay our field plots. The GEDI pre-launch plan included the development of a GEDI simulator that is able to reproduce the on-orbit GEDI data characteristics for the calibration of aboveground biomass models (Hancock et al., 2019). The simulation includes transforming discrete-return lidar point clouds into full-waveform signals (Blair and Hofton, 1999) in GEDI-sized footprints and with the expected GEDI instrument noise added. The waveform signal-to-noise ratio (SNR) on the on-orbit GEDI data depends on characteristics such as laser type (power or coverage), acquisition time (day or night), canopy cover and atmospheric conditions (Hancock et al., 2019; Dubayah et al., 2020; Duncanson et al., 2020). The simulator ensures consistency across point cloud flight characteristics especially for high-density lidar point clouds, as used as input in this study, that allow consistently transferring models to the on-orbit GEDI data. Complete description and validation of the GEDI simulator are described in detail in Hancock et al., 2019. GEDI-like waveforms were simulated from the high-density UAV-lidar point clouds clipped to the study sample plots using the *gediWFSimulator* tool in the rGEDI package (Silva et al., 2020) in R (R Core Team, 2020). Realistic noise was added considering a beam sensitivity of 0.98 (i.e., the canopy cover at which ground is detected 90% of the time with 5% probability of a false positive Hancock et al. (2019)) by using a link margin of 4.956 at 95% of canopy cover that relates to noise of the power beam collecting data at night (Boucher et al., 2020). For ground detection and metrics calculation, the waveforms were denoised and smoothed by setting the noise threshold as the mean plus 3 standard deviations and smoothing width (applied after denoising) equal to 0.5 m (Qi et al., 2019; Silva et al., 2021).

2.4.2. GEDI-derived vegetation structure metrics

We calculated the following metrics from the simulated GEDI full-waveforms (Table 2): RH (relative height) at the 98th height percentile (RH98, in m), canopy cover fraction (CCF, in %), plant area index (PAI, in m^2 m^{-2}), and Foliage Height Diversity (FHD, unitless). These metrics were selected to match to the GEDI Level 2A and 2B products and facilitate model interpretability. RH98 represents the height below which 98% of the returned laser energy is registered. It was selected to represent the top of the canopy, avoiding the noise of using the last return elevation value (Silva et al., 2018). The CCF is related to the percent of the ground covered by the vertical projection of canopy material calculated from the Gaussian fitted ground signal. PAI is the projected area of plant elements per unit ground surface, which relates

Table 2
GEDI waveform metrics used as predictors to estimate fuel load components.

Acronym	Description
RH98	Relative height at the 98th height percentile (m)
PAI	Plant Area Index (m^2 m^{-2})
CCF	Canopy cover fraction (%)
FHD	Foliage Height Diversity (unitless)

Fig. 3. GatorEye UAV-lidar (Gen 1) system. a) DJI M600 Pro hexacopter, with Phoenix Scout Ultra, hyperspectral, and visual sensors; b) three GNSS antennas for navigation, and one for sensor trajectory (positioned in the middle); c) Velodyne Ultra Puck lidar system.

to the canopy cover and plant occupation of the vertical space. The FHD is an index for expressing canopy structure complexity and vertical distribution (MacArthur and Horn, 1969). It is calculated by summing the product between the proportion of vertical PAI profiles and its logarithm in a selected horizontal layer (Tang and Armston, 2019). The theoretical basis and full description of cover and vertical profile GEDI metrics are detailed in the algorithm theoretical basis document (Tang and Armston, 2019). The metrics were calculated using the *gediWFMetrics* function in rGEDI (Silva et al., 2020) (Fig. 4).

2.5. Fuel load modeling development

Principal Component Analysis (PCA) was applied using the R package FactoMineR (Lê et al., 2008) for characterizing fuel load and GEDI metrics across field plots and vegetation formations. An explorative analysis of the derived PC scores was conducted in the first two components to analyze the relationships between field and GEDI variables.

Fuel loads were modeled separately, yielding five models with the GEDI metrics as predictors and SU_{fuels}, HB_{fuels}, SH_{fuels}, SS_{fuels}, WD_{fuels} and TF_{fuels} as response variables. We used the random forest (RF) algorithm implemented through the Caret R package (Kuhn et al., 2020) as our modeling approach. RF builds regression tree ensembles from bootstrapping the data, and the final prediction is the average ensemble outcome (Breiman et al., 1984; Breiman, 1996). This method was selected for being flexible to the different data distributions present in our dataset due to the various vegetation structures in the Cerrado formations (Fig. S1). Each RF was built with 500 trees tuning the number of predictors at each split (m_{try}). We tested m_{try} ranging from two to four ($2 \leq m_{try} \leq 4$), selecting the best tuned model in a 5-fold cross-validation assessment using the coefficient of determination (R^2), absolute (Mg ha^{-1}) and relative (%) root square mean error (RMSE) and mean difference (MD) (Eqs. 8 to 12).

$$R^2 = 1 - \frac{\sum_{i=1}^{n}\left(Y_i - \widehat{Y}_i\right)^2}{\sum_{i=1}^{n}\left(Y_i - \overline{Y}\right)^2} \tag{8}$$

$$RMSE\ (Mg/ha) = \sqrt{\frac{\sum_{i=1}^{n}\left(\widehat{Y}_i - Y_i\right)^2}{n}} \tag{9}$$

$$RMSE\ (\%) = \frac{RMSE}{\overline{Y}}\ x\ 100 \tag{10}$$

$$MD\ (Mg/ha) = \frac{\sum_{i=1}^{n}\left(\widehat{Y}_i - Y_i\right)}{n} \tag{11}$$

$$MD\ (\%) = \frac{MD}{\overline{Y}}\ x100 \tag{12}$$

where: $\widehat{Y}_i$is the estimated fuel load (Mg ha^{-1}), Y_i is the observed fuel load (Mg ha^{-1}); n is number of samples. For each fuel layer, the tuned model was run 500 times to account for the algorithm randomness.

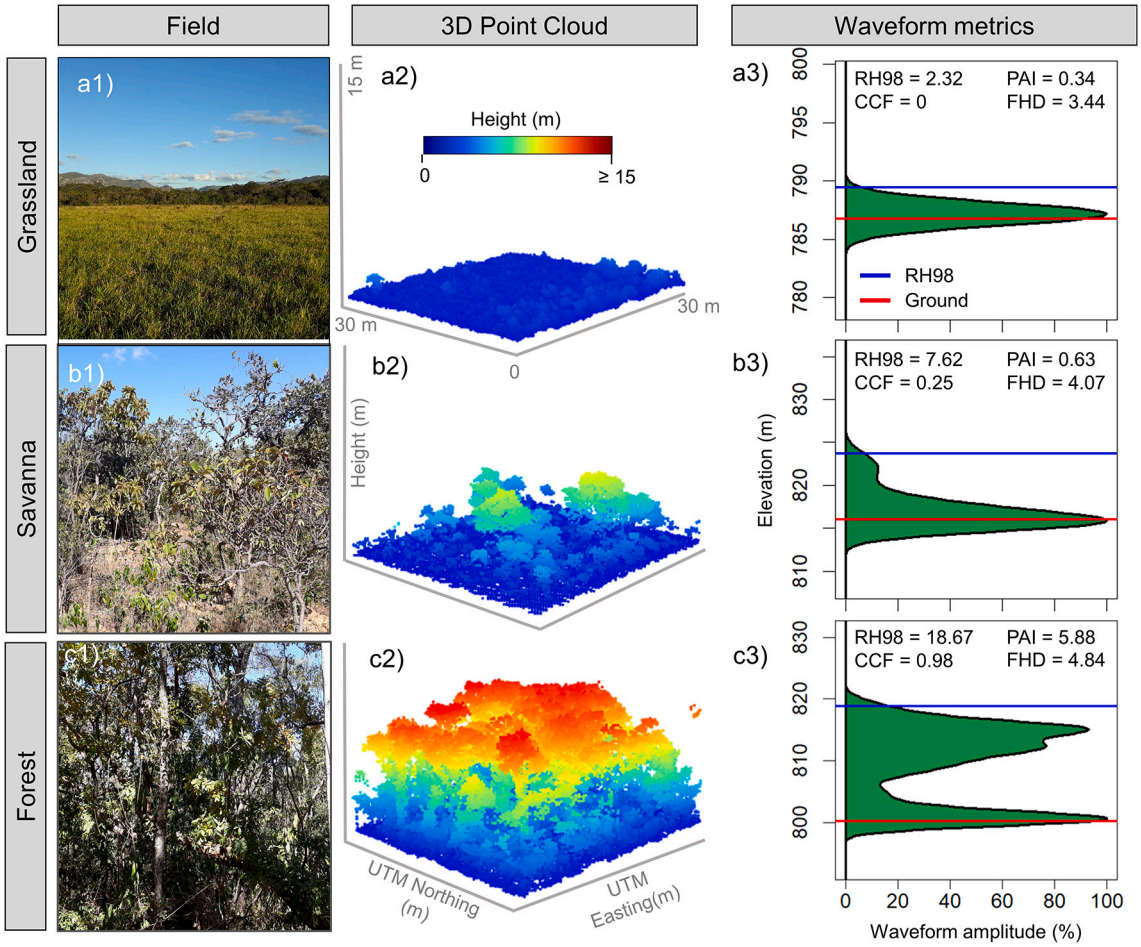

Fig. 4. Cerrado formations (a1, b1, and c1) and respective 3D point clouds from a UAV lidar survey (a2, b2, and c2) and metrics from the simulated waveforms (a3, b3, and c3).

2.6. Fuel loads characterization in Cerrado

The GEDI Level 2A and 2B version 2 data products (Dubayah et al., 2021a, 2021b) collected between April 18, 2019 and October 29, 2020 were downloaded over the entire Cerrado vegetated area. The GEDI orbits intersecting Cerrado limits were found and downloaded using the *gedifinder* and *gediDownload* functions in rGEDI package (Silva et al., 2020). The footprints were masked to the Cerrado vegetated area based on the land cover classification from Mapbiomas for the same year of the data collection (Souza et al., 2020). The GEDI footprint-level metrics (Table 2) were extracted using the *getLevel2AM* and *getLevel2B* functions and filtered using the quality flag (quality_flag = 1). This flag indicates usable data by summarizing individual quality assessment parameters based on waveform shot energy, sensitivity (< 0.9 over land), amplitude, and real-time surface tracking quality (Hofton and Blair, 2019; Beck et al., 2020).

The fuel load models developed in item 2.5 were applied to the GEDI footprints (diameter of ~25 m) collected across the Cerrado biome extent. Fuel load maps of each component were created by taking the average of the footprint-level estimates at 1-km^2 grid cells for mapping purposes and compatibility with planned gridded GEDI products (Dubayah et al., 2020) and requirements for global biomass maps (Hall et al., 2011).

We calculated the uncertainty of fuel load predictions in each cell by accounting for the footprints' variability within the cell, uncertainty associated with the RF algorithm, and RF lack of fit. To show this we start by assuming that the fuel load estimate at footprint i with model m is given:

$$RF_{im} = \theta_i + e_{im} \tag{13}$$

where θ_i is the overall mean prediction for footprint i and e_{im} is an error term. We assume that the expected value and variance of this error are E $[e_{im}] = 0$ and $Var[e_{im}] = \tau_i^2$, respectively. The parameter τ_i^2 captures the within-footprint variability associated with the randomness of the RF algorithm. We also assume that the RF mean prediction $\theta_i$is given by:

$$\theta_i = \mu_i + \epsilon_i \tag{14}$$

where μ_i is the true biomass of footprint i and $\epsilon_i$is another error term. This error term accounts for the fact that mean RF prediction is not identical to the true biomass. We assume that $E[\epsilon_i] = 0$ and $Var[\epsilon_i] = \psi^2$, where ψ^2 quantifies the uncertainty associated with the lack of fit of the RF model. These equations imply that:

$$RF_{im} = \mu_i + \epsilon_i + e_{im} \tag{15}$$

The fuel load prediction at footprint i is then given by the average of the RF models applied to footprint i:

$$\overline{RF}_i = \frac{\sum_m RF_{im}}{M} = \frac{M\mu_i}{M} + \frac{M\epsilon_i}{M} + \frac{\sum_m e_{im}}{M} = \mu_i + \epsilon_i + \frac{\sum_m e_{im}}{M} \tag{16}$$

where $\overline{RF}_i$ is the mean fuel load estimate at footprint i and M is the number of RF models that were fit. Assuming no correlation between lack of model fit (ϵ_i) and differences between RF models (e_{im}), this implies that:

$$Var\left(\overline{RF}_i | \mu_i\right) = \psi^2 + \frac{\tau_i^2}{M} \tag{17}$$

Recall that we took the average of all GEDI footprint-level fuel load predictions within a 1-km^2 cell. Assuming no spatial correlation in the mean fuel load in each footprint and model lack of fit, we have that the uncertainty associated with each cell is:

$$Var\left(\overline{RF}_k\right) = Var\left(\frac{\sum_i \overline{RF}_{ik}}{n_k}\right) = Var\left(\frac{\sum_i \mu_{ik}}{n_k} + \frac{\sum_i \epsilon_{ik}}{n_k} + \frac{\sum_i \frac{\sum_m e_{imk}}{M}}{n_k}\right) \tag{18}$$

where n_k is the number of GEDI footprints within the 1-km^2 cell (k).

If we assume that the uncertainty associated with model lack of fit (ψ^2) does not vary from footprint to footprint, then:

$$= Var\left(\frac{\sum_i \mu_{ik}}{n_k}\right) + Var\left(\frac{\sum_i \epsilon_{ik}}{n_k}\right) + Var\left(\frac{\sum_i \frac{\sum_m e_{imk}}{M}}{n_k}\right) \tag{19}$$

$$= Var\left(\frac{\sum_i \mu_{ik}}{n_k}\right) + \frac{n_k\psi^2}{n_k^2} + \frac{1}{n_k^2}\left(\sum_i \frac{M\tau_{ik}^2}{M^2}\right) \tag{20}$$

$$= Var\left(\frac{\sum_i \mu_{ik}}{n_k}\right) + \frac{\psi^2}{n_k} + \frac{\sum_i \tau_{ik}^2}{n_k^2 M} \tag{21}$$

Finally, if we assume that $E[\mu_{ik}] = m_k$ and $Var[\mu_{ik}] = \delta_k{}^2$, then the overall uncertainty at each cell (k) is given by:

$$= \frac{\delta_k^2}{n_k} + \frac{\psi^2}{n_k} + \frac{\sum_i \tau_{ik}^2}{n_k^2 M} \tag{22}$$

This expression shows that the variance for each cell k can be partitioned into the variability of biomass within each cell k (captured by $\delta_k{}^2$), model lack of fit (captured by ψ^2) and RF uncertainty (captured by $\tau_{ik}{}^2$). Notice that, as the number of GEDI footprints within cell k increases (i.e., n_k increases), then overall uncertainty decreases. Furthermore, increasing the number of RF models (i.e., M) only decreases the last uncertainty piece.

For each cell, we estimated $\delta_k{}^2$ and $\widehat{\tau}_{ik}^2$ with the following equations:

$$\widehat{\delta}_k^2 = \frac{\sum_i \left(\overline{RF}_{ik} - \overline{RF}_k\right)^2}{n_k - 1} \tag{23}$$

$$\widehat{\tau}_{ik}^2 = \frac{\sum_m \left(RF_{ikm} - \overline{RF}_{ik}\right)^2}{M - 1} \tag{24}$$

where $\overline{RF}_{ik}$ is the mean fuel load prediction of footprint i in cell k, $\overline{RF}_k$is the mean fuel load prediction in cell k, $\overline{RF}_{ikm}$is the fuel load prediction of footprint i in cell k using RF model m. The only variance parameter that is estimated separately using the field data is the lack of fit parameter (i.e., ψ^2). The estimation of this parameter is described in the supplementary material. The uncertainty is presented in absolute values by taking the square-root of the summed variance parameters. A workflow summarizing the full methodology applied in this study is provided in Fig. 5.

3. Results

3.1. Exploratory analysis of GEDI metrics and fuel components in the Cerrado formations

The PCA biplot shows distinct scores for the Cerrado formations and these first two PCs were responsible for 75.7% of the variables' cumulative variance (Fig. 6a). The RH98 and FHD showed high correlation with each other ($r = 0.94$, p-value = 2.2E-16) and were the two metrics mainly explaining the variability in PC1 being, overall, positively correlated to samples in the forest formation and negatively correlated with grassland observations. The fuel components that were mostcorrelated with RH98 and FHD were WD_{fuels} ($r > 0.85$ p-value <2.2E-15) and TF_{fuels} ($r > 0.82$, p-value <1.3E-13). SU_{fuels} had a weaker relationship ($r < 0.51$, p-value <0.0008) with the GEDI variables, though higher values were found in forests (Fig. 6b). Similarly, SH_{fuels} had lower correlations (r < |0.30|, p-value <0.03) with the GEDI variables than its sub-components SU_{fuels} ($r < 0.52$, p-value <0.0008) and HB_{fuels} (r < | 0.59|, p-value <0.002). The grassland observations showed opposite

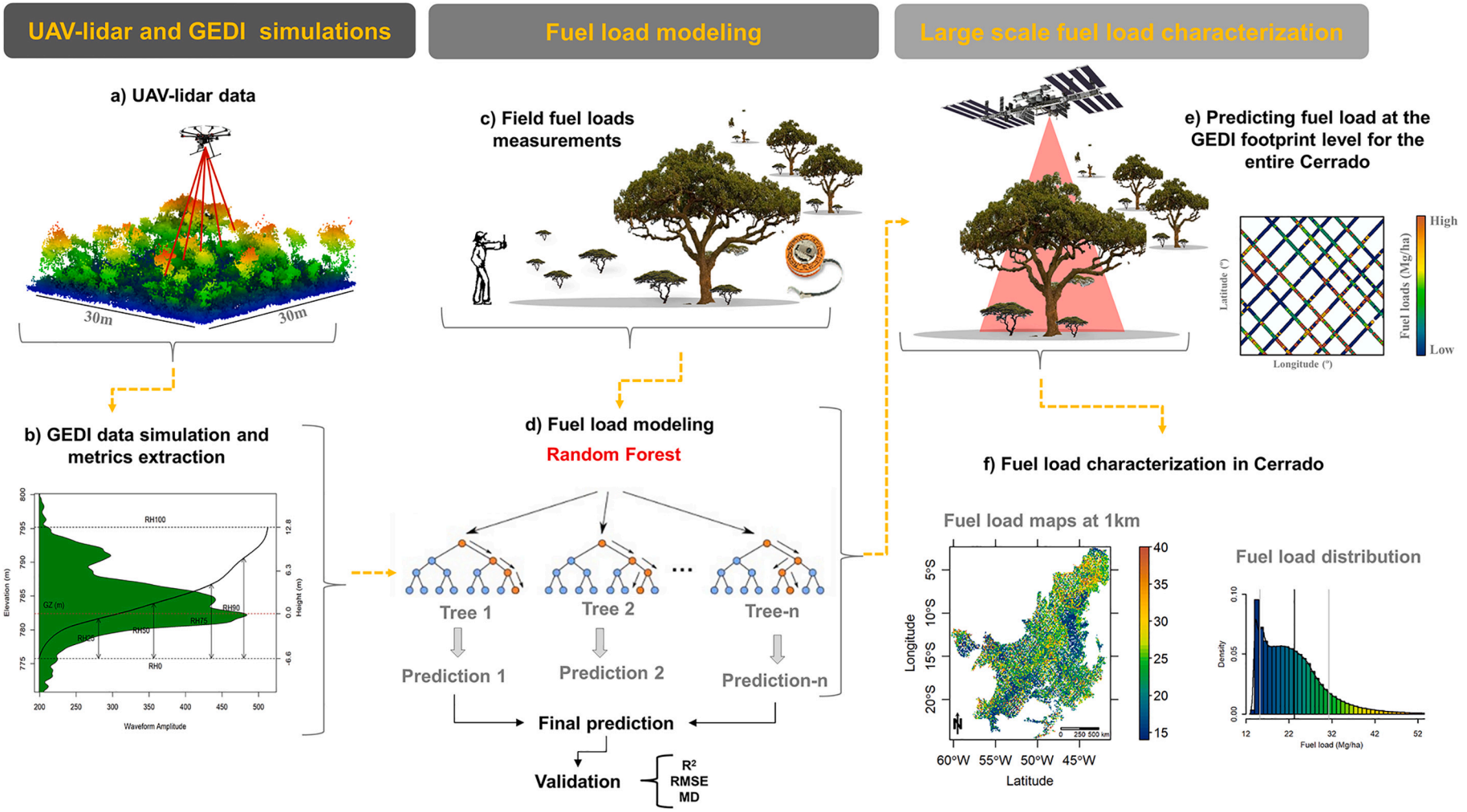

Fig. 5. Workflow to estimate fuel load components in Cerrado using GEDI data. High density UAV-lidar point clouds were collected (a) from which GEDI-like waveforms were simulated (b). The models were created using fuel load measurements from the field (c) as response variables in a random forest (RF) model and GEDI waveform metrics as predictors (d). The RF models were applied to the 25-m GEDI footprints in Cerrado (e) and averaged into 1-km grid cells (f).

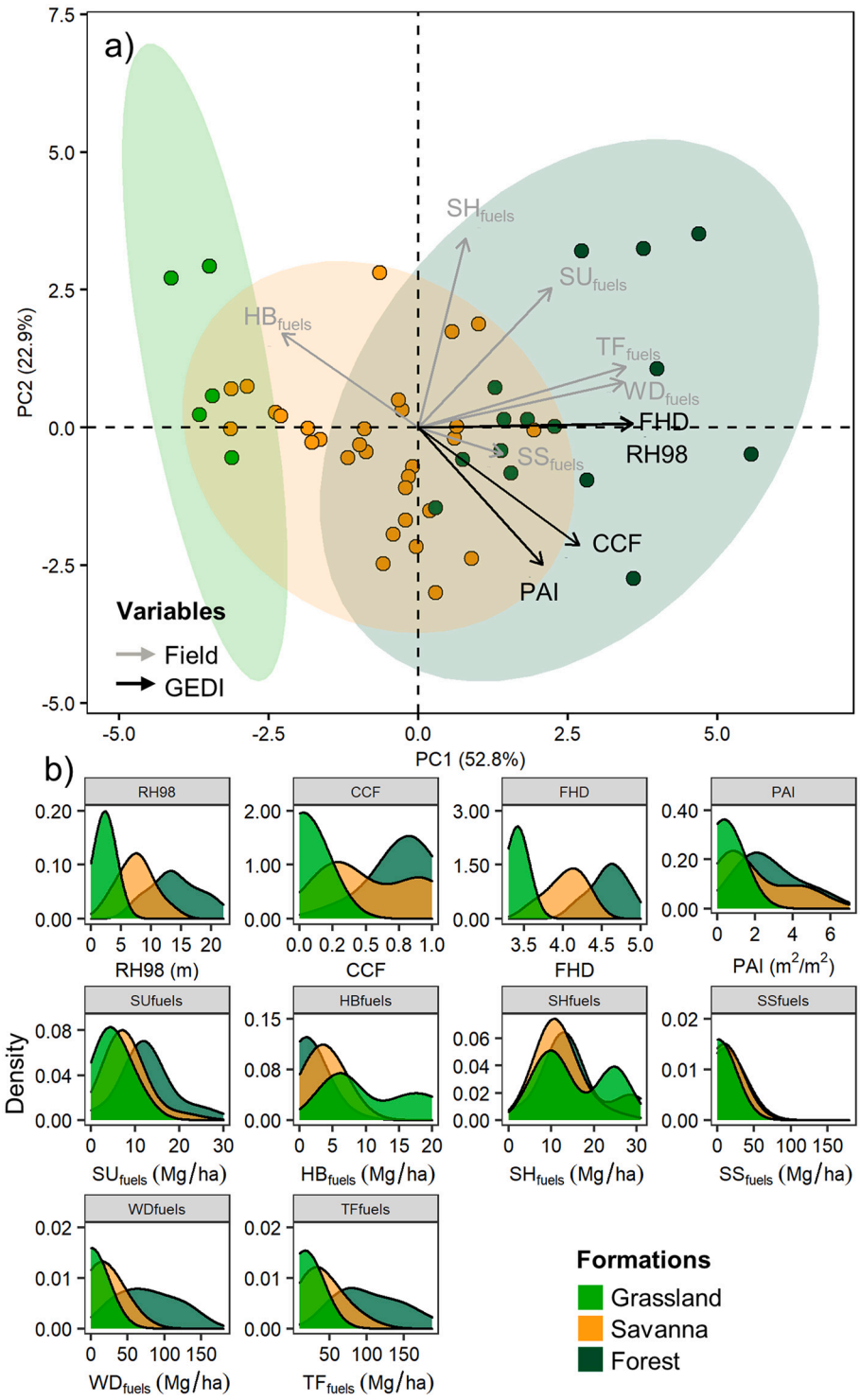

Fig. 6. Biplot of the first two axes of a principal component analysis of simulated GEDI waveforms metrics and field fuel load measurements (a) and their respective density plots (b). RH98 = Relative height at the 98 th height percentile; CCF = canopy cover fraction; FHD = Foliage Height Diversity; PAI = Plant Area Index; SU_{fuels} = surface fuels (duff, litter, downed wood); HB_{fuels} = Herbaceous fuels; SH_{fuels} = SU_{fuels} + HB_{fuels}; SS_{fuels} = shrubs and small trees (diameter at 1.3 m above ground (dbh) < 10 cm); WD_{fuels} = woody fuels (trees with dbh > 10 cm); TF_{fuels} = SU_{fuels} + HB_{fuels} + SS_{fuels} + WD_{fuels}.

scores on PC1 compared to the forest observations and were mostly represented by the variation in HB_{fuels}; this is consistent with the dominance of herbaceous species in these formations (Fig. S2) indicated by the negative correlation of HB_{fuels} with the metrics CCF and PAI. The savanna formation lies near the center, overlapping with the other two formations. This is also depicted in the variables' distributions (Fig. 6b), where most of the GEDI waveform metrics showed increasing values from grasslands to forests.

3.2. Fuel load models

Overall, all models presented relatively good performance during training with $R^2 > 0.78$, RMSE <10.83 Mg ha^{-1}, MD < 0.17 Mg ha^{-1} (Fig. 7). The WD_{fuels} and TF_{fuels} components were more accurately estimated with models, yielding R^2 values of 0.88 and 0.71, respectively, and RMSE of both ~40 Mg ha^{-1} in the validation (Table 3). On the other hand, the models estimating components at the lower stratum (SU_{fuels}, HB_{fuels}, SH_{fuels}) exhibited moderate to low performance during validation (R^2 < 0.46). The estimates were less accurate when estimating the

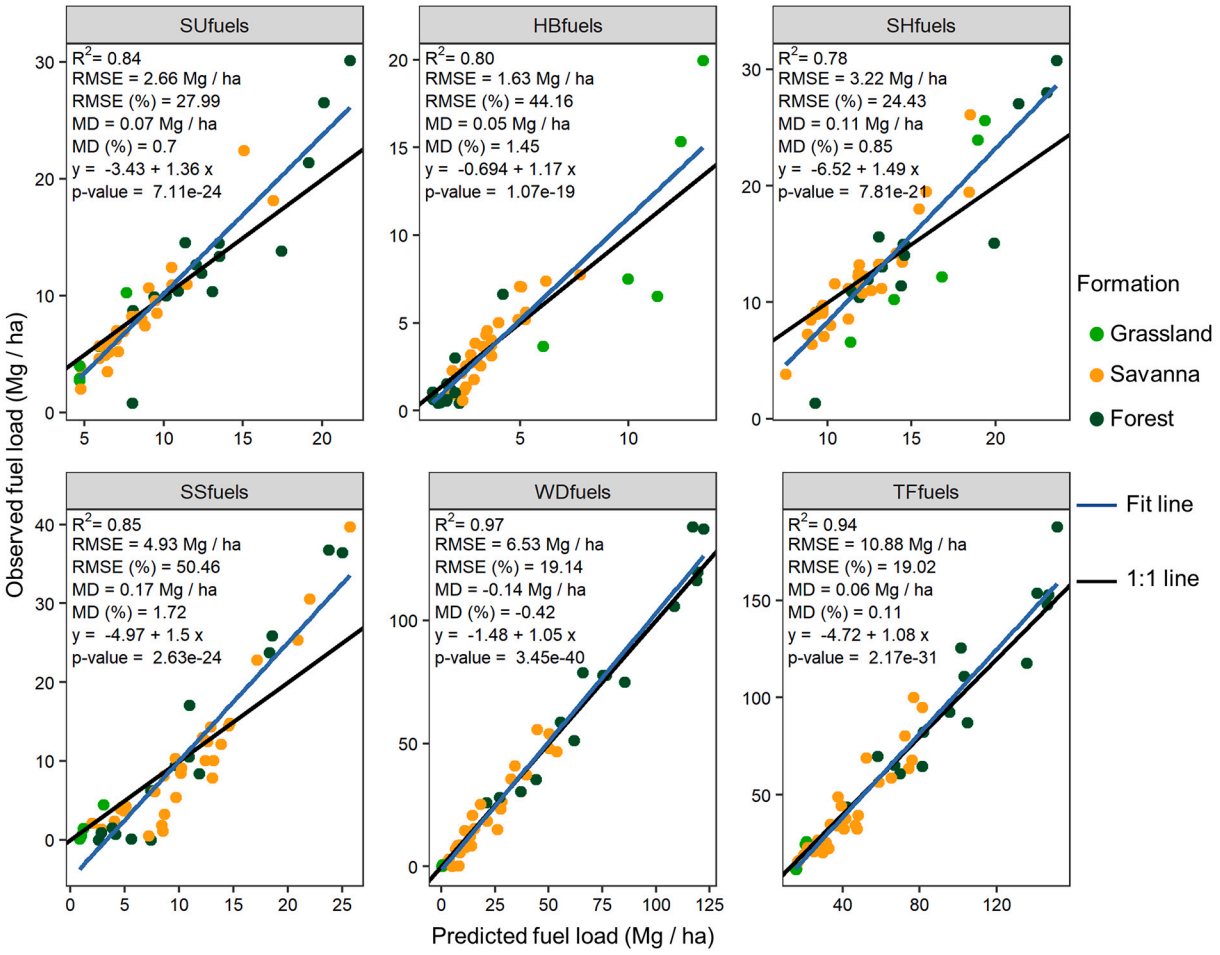

Fig. 7. Training results for estimating surface fuels (SU_{fuels}), herbaceous fuel (HB_{fuels}), surface and herbaceous fuels (SH_{fuels}), shrub (SS_{fuels}), tree (WD_{fuels}) and total fuel load (TF_{fuels}) using Random Forest and GEDI waveform metrics as predictors. R^2 = coefficient of determination; RMSE = root mean square error; and MD = mean difference.

Table 3
Cross-validation performance assessment in 500 iterations of models used to estimate surface fuels (SU_{fuels}), herbaceous fuel (HB_{fuels}), surface and herbaceous fuels (SH_{fuels}), shrub (SS_{fuels}), tree (WD_{fuels}) and total fuel load (TF_{fuels}). Values represent mean ± standard deviation.

Fuel	R^2	RMSE		MD	
		(Mg ha^{-1})	%	(Mg ha^{-1})	%
SU_{fuels}	0.31 ± 0.07	5.22 ± 0.21	55.51 ± 2.79	0.13 ± 0.18	4.61 ± 2.92
HB_{fuels}	0.46 ± 0.068	2.81 ± 0.2	78.6 ± 6.38	0.12 ± 0.14	10.01 ± 5.46
SH_{fuels}	0.17 ± 0.064	6.22 ± 0.34	47.49 ± 2.89	0.31 ± 0.28	4.04 ± 2.57
SS_{fuels}	0.15 ± 0.062	10.55 ± 0.5	113.32 ± 11.09	0.35 ± 0.35	16.01 ± 10.87
WD_{fuels}	0.88 ± 0.029	13.07 ± 0.67	40.6 ± 3.64	−0.32 ± 0.67	1.51 ± 2.83
TF_{fuels}	0.71 ± 0.052	23.01 ± 1.13	40.78 ± 2.4	0.22 ± 0.94	2.09 ± 2.12

R^2 = coefficient of determination; RMSE = root mean square error; and MD = mean difference.

surface and herbaceous components in a single model (i.e., SH_{fuels}; R^2 = 0.17, RMSE = 6.22 Mg ha^{-1}, MD = 0.31 Mg ha^{-1}) than in separate models; i.e., for HB_{fuels} (R^2 = 0.46, RMSE = 2.81 Mg ha^{-1}, MD = 0.12 Mg ha^{-1}) and for SU_{fuels} (R^2 = 0.31, RMSE = 5.22 Mg ha^{-1}, MD = 0.13 Mg ha^{-1}) individually. Differences in the training-validation performance were higher for SH_{fuels} and SS_{fuels}.

3.3. Fuel loads characterization across the Cerrado biome

Fuel load estimates were obtained from the application of the models to the on-orbit GEDI data. The estimates were obtained for the entire Cerrado biome in the 25 m-radii GEDI footprints. In a Cerrado subset (Fig. 8), gradients of fuel load associated with topography were observed in the different formations. For instance, there was a pattern of higher WD_{fuels} and TF_{fuels} estimates in forests (Fig. 8 e2 and f2) than in the other formations (Fig. 8 a2 - d2). On the other hand, HB_{fuels} estimates were significantly higher in grasslands (Fig. 8 a2), mainly when compared to forest formations (Fig. 8 e2 and f2). The SU_{fuels} estimates were also higher in forest formations (Fig. 8 e2 and f2) than in grasslands (Fig. 8 a2).

The spatial variation of fuel components estimates in Cerrado is shown in Fig. 9. These maps allowed us to identify regions in Cerrado with higher estimated HB_{fuels} and lower WD_{fuels} in some regions (e.g., ~45°W ~ 10°S, Fig. 9b and d) and regions with accumulated fuel as in northern Cerrado (e.g., ~45°W ~ 5°S Fig. 9e). The distribution of the estimates was mostly evenly distributed except for SH_{fuels} that was slightly skewed for higher values, and WD_{fuels} *and* TF_{fuels} that had higher frequencies of lower values (Fig. 10 a-f). The mean estimated values of SU_{fuels}, HB_{fuels}, SH_{fuels}, SS_{fuels}, WD_{fuels}, and TF_{fuels} were 7.63 ± 1.63, 7.87 ± 1.78, 14.74 ± 1.87, 7.58 ± 1.64, 10.29 ± 9.97 and 28.55 ± 11.4 Mg ha^{-1}, respectively. The uncertainty of the predictions was similarly distributed across Cerrado (Fig. 11), with a pattern of lower uncertainty

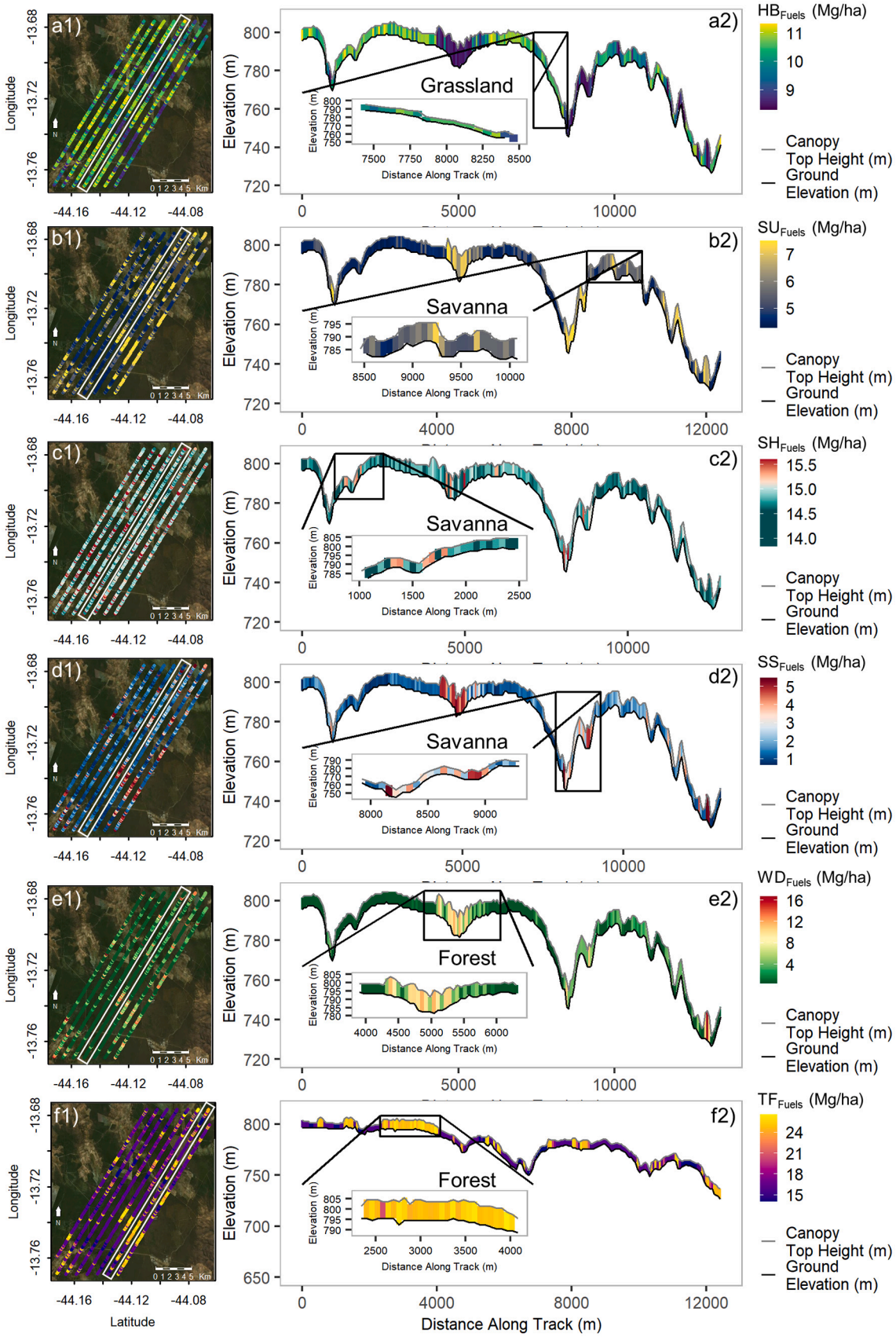

Fig. 8. Depiction of the GEDI footprint level estimates of fuel components showing all the GEDI ground-tracks (a1, b1, c1, d1, e1, f1) and a single-track profile over grassland, savanna, and forest formations (a2, b2, c2, d2, e2, f2). Estimates were done for surface fuels (SU_{fuels}), herbaceous fuels (HB_{fuels}), surface and herbaceous fuels (SH_{fuels}), shrubs and small trees (SS_{fuels}), woody fuels (WD_{fuels}) and total fuel load (TF_{fuels}).

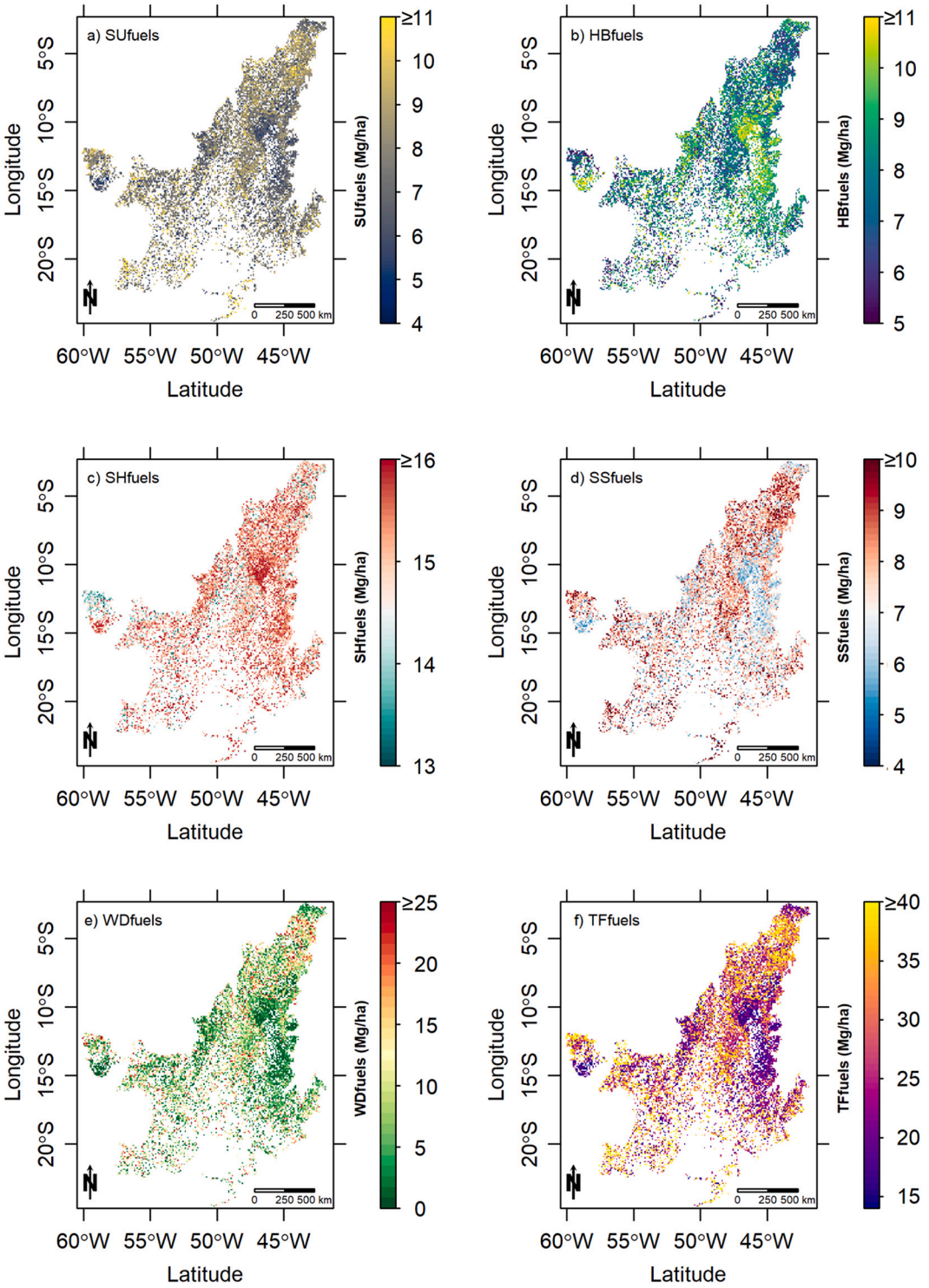

Fig. 9. GEDI-derived large scale fuel load estimates at the 1 km grid cell resolution for the entire Cerrado biome. These estimates were aggregated from the footprint-level predictions. Surface fuels (SU_{fuels} (a)), herbaceous fuels (HB_{fuels} (b)), surface and herbaceous fuels (SH_{fuels} (c)), shrubs and small trees fuels (SS_{fuels} (d)), woody fuels (WD_{fuels} (e)), and the total fuel load (TF_{fuels} (f)).

in regions with more GEDI footprints (Fig. S2).

4. Discussion

GEDI is capable of providing high resolution 3D canopy structural information of various forest ecosystems (Dubayah et al., 2020; Schneider et al., 2020) and holds untapped potential for establishing effective forest fire management frameworks. This study demonstrated the potential of using GEDI data to estimate large-scale multi-layer fuels across the whole Cerrado by applying both simulated and on-orbit data to model commonly used fuel load layers. The use of spaceborne lidar sensors for fuel mapping has been previously reported mainly to map canopy fuels with GLAS and ICESat-2 sensors (Ashworth et al., 2010; García et al., 2012; Peterson et al., 2013; Gwenzi et al., 2016; Narine et al., 2020). However, this is, to our knowledge, the first study demonstrating the usefulness of GEDI in estimating fuels loads at such a

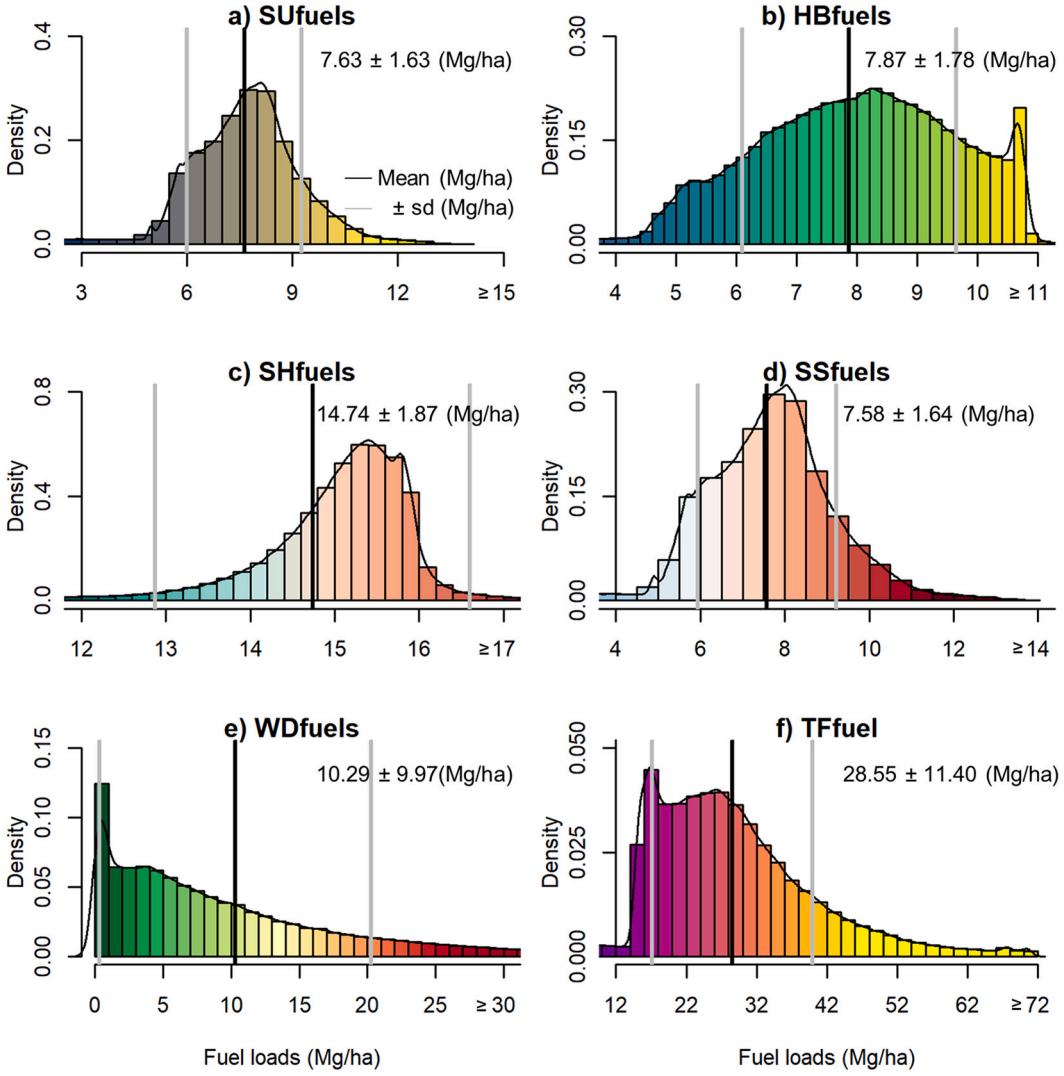

Fig. 10. Distribution of the estimates of fuel load components in Cerrado using GEDI waveform metrics and Random Forest. Separated models were trained to estimate surface fuels (SU_{fuels} (a)), herbaceous fuels (HB_{fuels} (b)), surface and herbaceous fuels (SH_{fuels} (c)), shrubs and small trees fuels (SS_{fuels} (d)), woody fuels (WD_{fuels} (e)), and the total fuel load (TF_{fuels} (f)).

large geographic scale, contributing to the expansion of spaceborne lidar applications for integrated fire management activities and supporting carbon monitoring initiatives in savannas.

4.1. Large scale fuel load estimation using spaceborne lidar

Our results demonstrated a high predictive capacity of GEDI metrics in modeling WD_{fuels} and TF_{fuels} that allows large-scale fuel load estimations. This finding is in agreement with similar studies focused on estimating biomass in different ecosystems using as predictors canopy metrics derived from spaceborne lidar sensors on the satellites ICESat-1 and ICESat-2 (Xiao et al., 2019). A study carried out by Lefsky et al. (2005) in a tropical broadleaf forest in Brazil demonstrated that GLAS-derived heights were able to explain 73% of the variation in field-measured aboveground biomass. Popescu et al. (2011), who mapped aboveground biomass in a temperate forest dominated by pine and oak stands in eastern Texas, found a strong relationship ($R^2 = 0.80$) between GLAS height variables and the reference biomass derived from airborne lidar data. In a more detailed study to test the capabilities of GLAS data in predicting forest aboveground biomass, Chi et al. (2015) estimated R^2 values ranging from 0.64 to 0.90 over different forest zones in China. Nevertheless, it is noteworthy that those studies did not account for important vegetation layers for fire management and that GLAS yield products at a coarser resolution (footprints with diameter of 70 m), despite being a full-waveform lidar as GEDI. Similarly, by using simulated ICESat-2 photon-counting lidar data, Narine et al. (2019) models explained 79% of the variation in AGB in a pine-dominated forest. Gwenzi et al. (2016) described some of the limitations of using ICESat-2 for retrieving vegetation height in structurally complex savannas. They found that canopy height estimation in areas of low-density vegetation cover may have lower precision due to the expected number of signal photons in these areas. The performance of our models also suggests that GEDI can be more appropriate for this type of vegetation.

Part of the unexplained variance by our SS_{fuels} models may be due to the lower sensitivity of GEDI to herbaceous and low stature shrubs compared to the denser overstory tree canopies the GEDI mission was designed to map. GEDI's utility for mapping short, sparse canopies and understory has yet to be established, and while the accuracies seen here are likely lower than for closed-canopy forests, or canopy fuels, our results suggest that GEDI data are still useful for this more challenging application. The measurement challenge is largely due to convolution of the waveform return from the ground and from short vegetation above the ground, where detecting the vegetation from the waveforms will be more challenging. This issue will be exacerbated over slopes or when

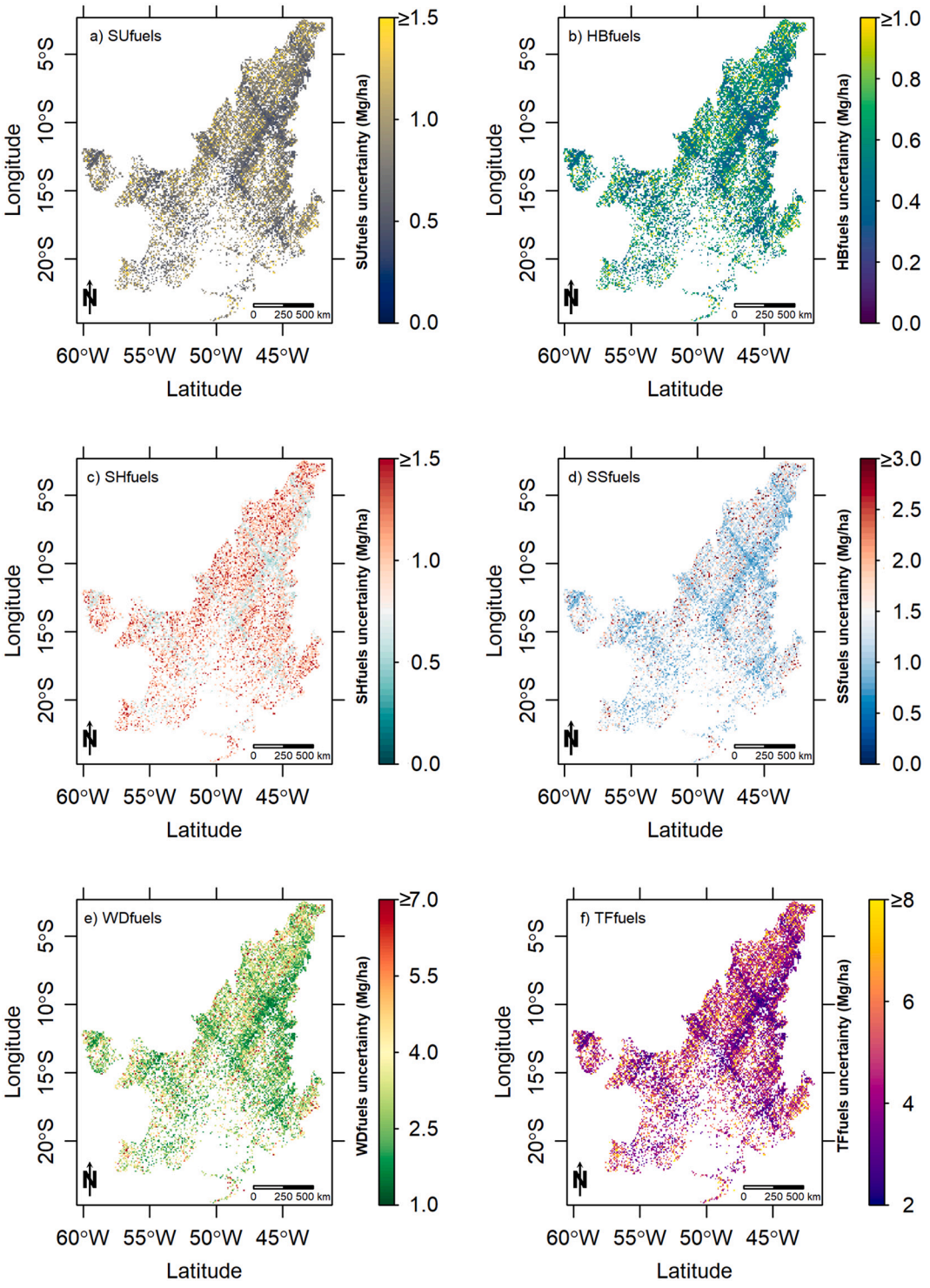

Fig. 11. Uncertainty of fuel load predictions accounting for the footprints' variability within the cell, uncertainty associated with the RF algorithm, and RF lack of fit. Surface fuels (SU_{fuels} (a)), herbaceous fuels (HB_{fuels} (b)), surface and herbaceous fuels (SH_{fuels} (c)), shrubs and small trees fuels (SS_{fuels} (d)), woody fuels (WD_{fuels} (e)), and the total fuel load (TF_{fuels} (f)).

vegetation cover is low, which is often the case in the Cerrado. The top portion of small trees and shrub crowns observed in the waveforms may not show enough canopy cover to register as a significant return signal and consequently may not be properly detected using the selected metrics.

Although surface, herbaceous and shrub fuels are a key component in fire behavior and emission models, most previous studies to estimate fuel loads using spaceborne lidar sensors focused on canopy fuels (García et al., 2012; Peterson et al., 2013). Obtaining information on fuels in low stature and sparse vegetation ecosystems, such as savannas and grasslands, is more challenging than in dense vegetation cover (e.g., Popescu et al., 2018). The lower performance for SU_{fuels}, HB_{fuels}, and SH_{fuels} suggests that spaceborne lidar data interacts with this lower stratum less strongly than with tree fuels. In fact, surface components are hardly directly retrieved with lidar measurements (Jakubowksi et al., 2013; Hudak et al., 2016b; Price and Gordon, 2016; Bright et al.,

2017), and it is commonly necessary to rely on their indirect relationship with other variables, such as canopy structure or climate (Hudak et al., 2016a; Mauro et al., 2021). Results in this study demonstrate that the GEDI waveform metrics could also be used as proxies to indirectly explain part of the variability of these fuels in savanna ecosystems and underscore the improvement in modeling HB_{fuels} and SU_{fuels} in separate models rather than a single model (SH_{fuels}). The difference among HB_{fuels} and SU_{fuels} is indicated by their contrasting relationships, such as having greater values of SU_{fuels} in forest formations (e.g., due to litterfall) and having inverse relationships to CCF and HB_{fuels}. Nonetheless, the dynamics of $HB_{fuels}$and SU_{fuels} may be more impacted than WD_{fuels} by plant phenology, seasonality (Costa et al., 2020; Oliveira et al., 2021), and fire events (Gomes et al., 2020b). Roitman et al. (2018) analyzed decades of AGB surveys in Cerrado and also demonstrated that environmental factors can help to explain part of the AGB variation in Cerrado. As more data become available, future studies could use multitemporal series to exploit the layers' seasonal structural dynamics mainly due to leaf flush and fall, in search for more unexplained variance that might not be obtained otherwise. The complementary use of multispectral and/or hyperspectral images for better distinguishing photosynthetic- from non-photosynthetic vegetation fractions (e.g., Roberts et al., 2003) coupled to GEDI metrics might improve the estimation of some surface fuels (e.g., litter, downed wood) in open-canopy formations and are recommended in future studies.

A multilevel approach by linking field plots, UAV-lidar, and spaceborne lidar data is the backbone of our methodological framework to produce both large scale multi-layer fuel load information in Cerrado. The RF models developed using simulated GEDI full-waveforms from UAV-lidar have the advantage of not being affected by waveform geolocation errors that are inherent with GEDI. Currently, these geolocation errors are around 10–20 m, but are expected to decrease to ~7–8 m after completed mission calibrations (Dubayah et al., 2020). This error can make it difficult to have coincident – in space and time - field and GEDI data for modeling. Our study is aligned with the simulation approach that has been suitable for GEDI model development and application (Saarela et al., 2018; Hancock et al., 2019; Marselis et al., 2019; Patterson et al., 2019; Qi et al., 2019; Schneider et al., 2020; Dubayah et al., 2020; Duncanson et al., 2020; Silva et al., 2021). Comprehensive assessments of the accuracy of on-orbit GEDI data in retrieving key structural vegetation parameters by synchronizing field measurements within GEDI footprints may be needed for assessing estimation uncertainty in different scales. Nevertheless, the models developed with simulated GEDI waveforms can be applied to the GEDI footprints covering about the entire globe (~52° N and S) providing a valuable asset for regional to global forest structure analysis as demonstrated for the Cerrado.

4.2. Caveats and source of uncertainty

While it may be straightforward to derive vegetation structural metrics in relatively dense vegetation cover (e.g., Popescu et al., 2018), obtaining such information in low stature and sparse vegetation formations, such as savannas and grasslands, is more challenging (Glenn et al., 2016; Gwenzi et al., 2016). One of the current limitations in our findings concerns the uncertainty of estimating surface and low stature vegetation fuels. This issue was also described in different studies using airborne lidar that reported R^2 ranging from ~25–45% (Jakubowksi et al., 2013, Hudak et al., 2016b, Price and Gordon, 2016, Bright et al., 2017). Pesonen et al. (2008) models had a better performance for estimating downed dead wood volume in boreal forests, suggesting a higher predictive capacity for this component. Nonetheless, despite surface fuels being a key component in fire behavior and emission models, they have received less attention than canopy fuels, particularly using spaceborne sensors (García et al., 2012; Peterson et al., 2013; Bright et al., 2017). Tackling this issue may require inclusion of variables related to fuel dynamics such as time since the last fire (Chen et al., 2017) and precipitation occurrence (Oliveira et al., 2021).

Another consideration is related to GEDI data characteristics. First, the GEDI mission is planned to collect data until 2023, limiting application of models to this time span. Nonetheless, we expect that other missions, such as MOLI (Murooka et al., 2013; Kimura et al., 2017; Asai et al., 2018), will give similar data in the future. The second point is related to the sampling nature of GEDI. We observed here that when aggregating footprints to a 1-km^2 grid cell there were still some areas not yet covered (Fig. S3), which can be due to the GEDI orbit missing the cells, or data loss from cloud cover. Those gaps might be filled with forthcoming dataset updates during the mission; it is expected that most 1 km^2 grid cells will have at least two ground tracks (Patterson et al., 2019) by the end of the GEDI mission lifetime. The number of required footprints to predict fuel load or AGB density in 1-km^2 cells may vary due to the vegetation complexity within the cell, which might need further investigation; nonetheless we observed an exponential decrease in uncertainty with an increase in number of footprints (Fig. S5). Finally, the impact of terrain characteristics for detecting ground and retrieving waveform metrics was not covered in this study. When the within footprint terrain slope is high, the interpretation of the signals is more complex causing, for instance, ground and canopy energy at the same height (Harding and Carabajal, 2005; Lefsky et al., 2005). In a study comparing small- and large-footprint lidar sensors, Silva et al. (2018) also observed an effect of terrain slope (> 20°) by overestimating ground elevation and RH metrics on large-footprint data, mainly in dense canopies. For instance, an alternative for GLAS waveforms was applying topographic correction using ancillary data (Lefsky et al., 2005; Lefsky et al., 2007). Similar effects of topography in the returned GEDI waveform may need to be investigated and addressed in further studies.

4.3. Future applications and challenges

Previous studies of GEDI have focused on deriving products by using the waveform metrics and its relationships with the vertical structure of the vegetation (Marselis et al., 2019; Schneider et al., 2020; Duncanson et al., 2020). The quality of the metrics relies on the accuracy to detect the ground signal which is expected to vary based on various factors such as canopy cover, GEDI beam energy, weather conditions and topography. However, apart from the environmental characteristics and sensor properties, what determines the ground classification is the algorithm incorporated. Hancock et al. (2019) described and tested Gaussian fitting along with the lowest maximum and inflection point algorithms to detect the ground signal and calculated RH metrics from simulated GEDI waveforms, showing that there might be differences among them. Further research exploring the impact of ground algorithms on GEDI metrics associated with fuel load estimation needs to be conducted, ideally with the study based on individual physiognomies and landscape conditions.

RF was implemented in our study due to its ease of usage, interpretability, versatility in handling missing data, and prior success with respect to fuel load estimation and to GEDI-based studies (Healey et al., 2020; Marshak et al., 2020; Rishmawi et al., 2021). Being an ensemble technique, RF improves the average prediction performance and is robust to outliers. Techniques such as ordinary least square regression, lasso logistic regressions and sensitivity analysis, and combinations of multiple machine learning methods, have also been applied to GEDI data for quantifying forest traits and structural diversity (Boucher et al., 2020; Burns et al., 2020; Duncanson et al., 2020; Sanchez-Lopez et al., 2020). More recently, deep learning-based regression models, e.g., Convolutional Neural Networks (CNN), have been successfully applied for estimating continuous forest structural parameters such as AGB (Asner et al., 2018) and canopy height (Lang et al., 2019; Li et al., 2020). For instance, Li et al. (2020) showed that deep learning slightly outperforms random forest models in the estimate of canopy height. Therefore, a review of the efficiency of various statistical modeling techniques for the estimation of disparate forest metrics can be deemed

to be a critical step for furthering GEDI powered research for fuel load and AGB modeling and management.

With several planned global missions, such as NASA-ISRO's NISAR and ESA's BIOMASS, offering new capabilities, data fusion of GEDI with these distinct sensors can compensate for drawbacks such as influence of clouds, atmospheric haze, multiple scattering, sloped terrain and off-nadir pointing (Pardini et al., 2019; Yang et al., 2011; Quegan et al., 2019; Rosen et al., 2015). We also encourage readers to take full advantage of the Multi-Mission Algorithm and Analysis Platform (MAAP) that hosts a colossal amount of related data, tools, algorithms, and computing capabilities for performing multi-sensor operations (Albinet et al., 2019). During the initial phase of GEDI, several studies had explored the possibility of merging GEDI with synthetic aperture radar (SAR) for improving various forest metrics such as forest height and other structure attribute mapping and characterization (Qi et al., 2019; Qi and Dubayah, 2016). Adding to this, a study by Silva et al. (2021) highlighted how integrating NISAR and ICESat-2 with GEDI offer us new opportunities for enhancing AGB mapping in temperate forests with complex terrain. Similarly, data from multispectral sensors also hold potential for improving spatial resolution of GEDI (Potapov et al., 2021). Such multi-sensor data fusion approaches will be important for developing wall-to-wall maps in applications that require higher spatial resolution such as fire behavior models (Benali et al., 2016; Saatchi et al., 2007). Data fusion approaches applicability for estimating large scale forest canopy height, AGB and past forest disturbances assessment has been already demonstrated (Potapov et al., 2021; Saarela et al., 2018; Sanchez-Lopez et al., 2020). Ultimately, data integration from different missions (e.g., NASA's Landsat 8/OLI and NISAR, and ESA's Sentinel 2/MSI and BIOMASS) will be necessary for developing wall-to-wall maps with finer spatial resolutions and for covering regions outside GEDI orbit coverage.

Fuel mapping is one of the most important stages that should be considered in wildfire prevention and planning (Keane and Reeves, 2012; Agee and Skinner, 2005; Franke et al., 2018). With the proposed framework it is possible to obtain fuel load estimates for large areas, such as the Cerrado biome. This is a key point for advancing on a broad spatial scale understanding of fire effects on ecological processes, ecosystem functioning, carbon emissions, and fuel dynamics (Turner et al., 1995; Bowman et al., 2013; Gomes et al., 2018; Oliveira et al., 2021). Management solutions based on integrated fire management initiatives have taken place in Cerrado conservation areas mainly since 2014 and consider practices of prescribed burning in mosaics to preserve the fire history of a region (Schmidt et al., 2018). The fuel components estimate for large areas as developed here will also be an important resource for this end (Franke et al., 2018; Gomes et al., 2018; Schmidt et al., 2018).

5. Conclusions

In this study we evaluated the capability of GEDI data for estimating large scale multi-layer fuel loads in a tropical savanna ecosystem. We used the random forest algorithm fed by GEDI waveform metrics simulated from high-density UAV-lidar 3D point clouds as our modeling approach. To our knowledge, this is the first attempt to map different fuel components with GEDI waveform metrics. Overall, the models had better performance for predicting woody fuels (e.g., WD_{fuels} and TF_{fuels}). Our results support the expected benefits of using GEDI data for improving models to estimate vegetation traits on structurally-complex ecosystems. Furthermore, we were able to upscale from local to biome-level predictions by applying our models to GEDI data over the entire Cerrado yielding relatively high-resolution fuel load estimates in this region. Therefore, we expect that users can potentially improve large-scale fuel load monitoring using the presented framework and extend the analysis to other fire-prone ecosystems. Following research on data integration of GEDI data with different sensors is expected for meeting spatial and temporal requirements of other fire-related applications - such as assessing fuel load dynamics, modeling fire behavior and calculating carbon emissions - and assist in better understanding the climate-fire interactions across different landscapes.

Declaration of Competing Interest

The authors declare that they have no known competing financial interests or personal relationships that could have appeared to influence the work reported in this paper.

Acknowledgements

This project was supported by the Brazilian National Council for Scientific and Technological Development (CNPq, grant 442640/2018-8, CNPq/Prevfogo-Ibama N° 33/2018). D.R.A.A. was supported by the São Paulo Research Foundation (#2018/21338-3). This study was financed in part by the Coordenação de Aperfeiçoamento de Pessoal de Nível Superior – Brasil (CAPES) – Finance Code 001. A.P.D.C. was financed in part by MCTIC/CNPq N° 28/2018 (#408785/2018-7; #438875/2018-4, #313887/2018-7). V.L., received individual CNPq grant (#315699/2020-5). M.P·F was supported by CNPq grant 306345/2020-0. R.V.L. was supported by CAPES (#88887.463733/2019-00). We gratefully acknowledge the following undergraduate and graduate students involved in the field work campaign: Alberto A. Gontijo e Silva, Alexandre S. C. Filho, André Felipe C. Lima, Bernardo dos S. de Almeida, Carlos Magno M. de Oliveira, Gilberto do A. Pacheco; Gustavo R. Lattanzi, Iago Henrique F. da Silva, Irene M. Barbosa, Ivo S. Moreira, Jacson A. A. Machado, Jean Victor N. Paiva, Junia S. M. Macedo, Leandra Dietrich, Lídia A. de Aguiar, Matheus Gunther M. Soares, Nelson Amaral, Nivaldo R. J. Junior, Reginaldo Arthur G. Marcelino, Thiago Trajano, Victor Almeida Cordeiro. Moreover, we thank the park managers: Edward Elias Junior, Celso Lago-Paiva and Leandro Chagas from the Serra do Cipó National Park, Maria Carolina A. Camargos from the Chapada dos Veadeiros National Park and Renato Diniz Dumont from the Paraopeba National Forest. GatorEye data collection and processing by AMAZ and ENB was supported in part by the McIntire-Stennis program of the USDA, and the School of Forest Resources and Conservation and the Center for Latin America Studies at UFL.

Author contributions

R.V.L., C.A.S., and C.K. designed the study. M.B.T.C., A.L.S., L.R.R.Y. G., D.R.A.A., G.E.M., A.H., and C.K. collected and processed the field data. E.N.B., and A.M.A.Z. collected and processed the UAV-lidar data. C.H.A., E.A.T.M. M.M., C.H., R.V., B.L.F., C.H.L.S.J., J.L., B.A.F.M., S.H., D.V., and A.C., contributed with the methodological framework, data processing analysis and write up. C.A.S., C.K., A.T.H., S.G., D.R.A.A., V. L., A.P.D.C., P.H.S·B, B.A.F.M., L.E.O.C.A., M.G., T.M., S.S., S.H., L.D., M. P·F, D.V., and J.X. contributed to the interpretation, quality control and revisions of the manuscript. All authors read and approved the final version of the manuscript.

Appendix A. Supplementary data

Supplementary data to this article can be found online at https://doi.org/10.1016/j.rse.2021.112764.

References

Agee, J.K., Skinner, C.N., 2005. Basic principles of forest fuel reduction treatments. For. Ecol. Manag. 211 (1–2), 83–96. https://doi.org/10.1016/j.foreco.2005.01.034.

Albinet, C., Whitehurst, A.S., Jewell, L.A., Bugbee, K., Laur, H., Murphy, K.J., Duncanson, L., 2019. A joint ESA-NASA multi-mission algorithm and analysis platform (MAAP) for biomass, NISAR, and GEDI. Surv. Geophys. 40 (4), 1017–1027.

Andela, N., Morton, D.C., Giglio, L., Chen, Y., Van Der Werf, G.R., Kasibhatla, P.S., DeFries, R.S., Collatz, G.J., Hantson, S., Kloster, S., Bachelet, D., Forrest, M., Lasslop, G., Li, F., Mangeon, S., Melton, J.R., Yue, C., Randerson, J.T., 2017.

A human-driven decline in global burned area. Science 356 (6354), 1356–1362. https://doi.org/10.1126/science.aal4108.
Andela, N., Morton, D.C., Chen, Y., Giglio, L., Randerson, J.T., 2018. A global fire atlas of size, duration, and spread from satellite burned area data. In: EGU General Assembly Conference Abstracts, p. 11269.
Asai, K., Hirata, Y., Takao, G., Simoda, H., Honda, Y., Kajiwara, K., Awaya, Y., 2018. MOLI (multi-footprintobservation lidar and imager) mission for globally observing forest canopy height and forest structural characteristics from ISS (International Space Station)-JEM (Japanese Experimental Module). In: JpGU Meeting: Chiba, Japan. May 20–24.
Ashworth, A., Evans, D.L., Cooke, W.H., Londo, A., Collins, C., Neuenschwander, A., 2010. Predicting southeastern forest canopy heights and fire fuel models using GLAS data. Photogramm. Eng. Remote. Sens. 76 (8), 915–922.
Asner, G.P., Brodrick, P.G., Philipson, C., Vaughn, N.R., Martin, R.E., Knapp, D.E., Heckler, J., Evans, L.J., Jucker, T., Goossens, B., Stark, D.J., Reynolds, G., Ong, R., Renneboog, N., Kugan, F., Coomes, D.A., 2018. Mapped aboveground carbon stocks to advance forest conservation and recovery in Malaysian Borneo. Biol. Conserv. 217, 289–310. https://doi.org/10.1016/j.biocon.2017.10.020.
Beck, J., Armston, J., Hofton, M., Luthcke, S., 2020. Global Ecosystem Dynamics Investigation (GEDI) Level 02 User Guide. Version 1.0. https://lpdaac.usgs.gov/documents/650/GEDI02_UserGuide_V1.pdf. (Accessed 13 March 2021).
Benali, A., Ervilha, A.R., Sá, A.C.L., Fernandes, P.M., Pinto, R.M.S., Trigo, R.M., Pereira, J.M.C., 2016. Deciphering the impact of uncertainty on the accuracy of large wildfire spread simulations. Sci. Total Environ. 569, 73–85. https://doi.org/10.1016/j.scitotenv.2016.06.112.
Blair, J.B., Hofton, M.A., 1999. Modeling laser altimeter return waveforms over complex vegetation using high-resolution elevation data. Geophys. Res. Lett. 26 (16), 2509–2512. https://doi.org/10.1029/1999GL010484.
Boucher, P.B., Hancock, S., Orwig, D.A., Duncanson, L., Armston, J., Tang, H., Schaaf, C., 2020. Detecting change in forest structure with simulated GEDI lidar waveforms: A case study of the hemlock woolly Adelgid (HWA; Adelges tsugae) infestation. Remote Sens. 12 (8), 1304. https://doi.org/10.3390/rs12081304.
Bowman, D.M., O'Brien, J.A., Goldammer, J.G., 2013. Pyrogeography and the global quest for sustainable fire management. Annu. Rev. Environ. Resour. 38, 57–80. https://doi.org/10.1146/annurev-environ-082212-134049.
Breiman, L., 1996. Some properties of splitting criteria. Mach. Learn. 24 (1), 41–47. https://doi.org/10.1023/A:1018094028462.
Breiman, L., Friedman, J., Stone, C.J., Olshen, R.A., 1984. Classification and Regression Trees. CRC press.
Bright, B.C., Hudak, A.T., Meddens, A.J., Hawbaker, T.J., Briggs, J.S., Kennedy, R.E., 2017. Prediction of forest canopy and surface fuels from lidar and satellite time series data in a bark beetle-affected forest. Forests 8 (9), 322. https://doi.org/10.3390/f8090322.
Broadbent, E.N., Zambrano, A.M.A., Omans, G., Adler, A., Alonso, P., Naylor, D., Chenevert, G., Murtha, T., Vogel, J., Almeida, D.R.A., Dalla Corte, A.P., Silva, C.A., Prata, G.A., Merrick, T., D'Oliveira, M.V.N., Detto, M., Ferreira, M.P., Wilkinson, B. E., Ferreira, M.E., Muller-Landau, H.C., 2021. The GatorEye Unmanned Flying Laboratory: Sensor Fusion for 4D Ecological Analysis Through Custom Hardware and Algorithm Integration. accessed Feb 10 2021. Retrieved from. http://www.gatoreye.org.
Burns, P., Clark, M., Salas, L., Hancock, S., Leland, D., Jantz, P., Goetz, S.J., 2020. Incorporating canopy structure from simulated GEDI lidar into bird species distribution models. Environ. Res. Lett. 15 (9), 095002 https://doi.org/10.1088/1748-9326/ab80ee.
Chave, J., Réjou-Méchain, M., Búrquez, A., Chidumayo, E., Colgan, M.S., Delitti, W.B., Vieilledent, G., 2014. Improved allometric models to estimate the aboveground biomass of tropical trees. Glob. Chang. Biol. 20 (10), 3177–3190. https://doi.org/10.1111/gcb.12629.
Chen, L., Yang, J., Kong, H., 2017. Lidar-histogram for fast road and obstacle detection. In: 2017 IEEE International Conference on Robotics and Automation (ICRA). IEEE, pp. 1343–1348. https://doi.org/10.1109/ICRA.2017.7989159.
Chi, H., Sun, G., Huang, J., Guo, Z., Ni, W., Fu, A., 2015. National Forest Aboveground Biomass Mapping from ICESat/GLAS data and MODIS imagery in China. Remote Sens. 7 (5), 5534–5564. https://doi.org/10.3390/rs70505534.
Chuvieco, E., Aguado, I., Cocero, D., Riano, D., 2003. Design of an empirical index to estimate fuel moisture content from NOAA-AVHRR images in forest fire danger studies. Int. J. Remote Sens. 24 (8), 1621–1637. https://doi.org/10.1080/01431160210144660b.
Chuvieco, E., Aguado, I., Salas, J., García, M., Yebra, M., Oliva, P., 2020. Satellite remote sensing contributions to wildland fire science and management. Curr. Forest. Rep. 6 (2), 81–96. https://doi.org/10.1007/s40725-020-00116-5.
Costa, A.N., Souza, J.R., Alves, K.M., Penna-Oliveira, A., Paula-Silva, G., Becker, I.S., Marinho-Vieira, K., Bonfim, A.L., Bartimachi, A., Vieira-Neto, E.H.M., 2020. Linking the spatiotemporal variation of litterfall to standing vegetation biomass in Brazilian savannas. J. Plant Ecol. 13, 517–524. https://doi.org/10.1093/jpe/rtaa039.
da Costa, M.B.T., Silva, C.A., Broadbent, E.N., Leite, R.V., Mohan, M., Liesenberg, V., Stoddart, J., Amaral, C.H., Almeida, D.R.A., Silva, A.L., Goya, L.R.R.Y., Cordeiro, V. A., Rex, F., Hirsch, A., Marcatti, G.E., Cardil, A., Mendonça, B.A.F., Hamamura, C., Dalla Corte, A.P., Matricardi, E.A.T., Hudak, A.T., Zambrano, A.M.A., Valbuena, R., Faria, B.L., Junior, C.H.L.S., Aragão, L., Ferreira, M.E., Liang, J., Carvalho, S.P.C., Klauberg, C., 2021. Beyond trees: mapping total aboveground biomass density in the Brazilian savanna using high-density UAV-lidar data. For. Ecol. Manag. 491. https://doi.org/10.1016/j.foreco.2021.119155.
Dubayah, R., Blair, J.B., Goetz, S., Fatoyinbo, L., Hansen, M., Healey, S., Hofton, M., Hurtt, G., Kellner, J., Luthcke, S., Armston, J., Tang, H., Duncanson, L., Hancock, S., Jantz, P., Marselis, S., Patterson, P.L., Qi, W., Silva, C., 2020. The global ecosystem dynamics investigation: high-resolution laser ranging of the Earth's forests and topography. Sci. Remote Sens. 1, 100002. https://doi.org/10.1016/j.srs.2020.100002.
Dubayah, R., M. Hofton, J. Blair, J. Armston, H. Tang, S. Luthcke. GEDI L2A Elevation and Height Metrics Data Global Footprint Level V002. 2021a, distributed by NASA EOSDIS Land Processes DAAC, https://doi.org/10.5067/GEDI/GEDI02_A.002. Accessed 2021-08-29.
Dubayah, R., H. Tang, J. Armston, S. Luthcke, M. Hofton, J. Blair. GEDI L2B Canopy Cover and Vertical Profile Metrics Data Global Footprint Level V002. 2021b, distributed by NASA EOSDIS Land Processes DAAC, https://doi.org/10.5067/GEDI/GEDI02_B.002. Accessed 2021-08-29.
Duncanson, L.I., Niemann, K.O., Wulder, M.A., 2010. Estimating forest canopy height and terrain relief from GLAS waveform metrics. Remote Sens. Environ. 114 (1), 138–154. https://doi.org/10.1016/j.rse.2009.08.018.
Duncanson, L., Neuenschwander, A., Hancock, S., Thomas, N., Fatoyinbo, T., Simard, M., Dubayah, R., 2020. Biomass estimation from simulated GEDI, ICESat-2 and NISAR across environmental gradients in Sonoma County, California. Remote Sens. Environ. 242, 111779. https://doi.org/10.1016/j.rse.2020.111779.
Durigan, G., Ratter, J.A., 2016. The need for a consistent fire policy for Cerrado conservation. J. Appl. Ecol. 53 (1), 11–15. https://doi.org/10.1111/1365-2664.12559.
Durigan, G., Pilon, N.A., Abreu, R.C., Hoffmann, W.A., Martins, M., Fiorillo, B.F., Vasconcelos, H.L., 2020. No net loss of species diversity after prescribed fires in the Brazilian savanna. Front. Forests Glob. Change 3, 13. https://doi.org/10.3389/ffgc.2020.00013.
Erdody, T.L., Moskal, L.M., 2010. Fusion of LiDAR and imagery for estimating forest canopy fuels. Remote Sens. Environ. 114 (4), 725–737. https://doi.org/10.1016/j.rse.2009.11.002.
Ferreira, L.G., Urban, T.J., Neuenschawander, A., De Araújo, F.M., 2011. Use of orbital LIDAR in the Brazilian Cerrado biome: potential applications and data availability. Remote Sens. 3 (10), 2187–2206. https://doi.org/10.3390/rs3102187.
Franke, J., Barradas, A.C.S., Borges, M.A., Menezes Costa, M., Dias, P.A., Hoffmann, A.A., Orozco Filho, J.C., Melchiori, A.E., Siegert, F., 2018. Fuel load mapping in the Brazilian Cerrado in support of integrated fire management. Remote Sens. Environ. 217, 221–232. https://doi.org/10.1016/j.rse.2018.08.018.
Gajardo, J., García, M., Riaño, D., 2014. Applications of airborne laser scanning in Forest fuel assessment and fire prevention. In: Maltamo, M., Næsset, E., Vauhkonen, J. (Eds.), Forestry Applications of Airborne Laser Scanning: Concepts and Case Studies. Springer Netherlands, Dordrecht, pp. 439–462.
García, M., Popescu, S., Riaño, D., Zhao, K., Neuenschwander, A., Agca, M., Chuvieco, E., 2012. Characterization of canopy fuels using ICESat/GLAS data. Remote Sens. Environ. 123, 81–89. https://doi.org/10.1016/j.rse.2012.03.018.
García, M., Saatchi, S., Casas, A., Koltunov, A., Ustin, S.L., Ramirez, C., Balzter, H., 2017. Extrapolating forest canopy fuel properties in the California rim fire by combining airborne LiDAR and landsat OLI data. Remote Sens. 9, 1–18. https://doi.org/10.3390/rs9040394.
Glenn, N.F., Neuenschwander, A., Vierling, L.A., Spaete, L., Li, A., Shinneman, D.J., McIlroy, S.K., 2016. Landsat 8 and ICESat-2: performance and potential synergies for quantifying dryland ecosystem vegetation cover and biomass. Remote Sens. Environ. 185, 233–242. https://doi.org/10.1016/j.rse.2016.02.039.
Gomes, L., Miranda, H.S., Bustamante, M. M. da C., 2018. How can we advance the knowledge on the behavior and effects of fire in the Cerrado biome? For. Ecol. Manag. 417, 281–290. https://doi.org/10.1016/j.foreco.2018.02.032.
Gomes, L., Miranda, H.S., Silvério, D.V., Bustamante, M.M.C., 2020a. Effects and behaviour of experimental fires in grasslands, savannas, and forests of the Brazilian Cerrado. For. Ecol. Manag. 458, 117804. https://doi.org/10.1016/j.foreco.2019.117804.
Gomes, L., Miranda, H.S., Soares-Filho, B., Rodrigues, L., Oliveira, U., Bustamante, M.M. C., 2020b. Responses of plant biomass in the Brazilian savanna to frequent fires. Front. Forests Glob. Change 3, 1–11. https://doi.org/10.3389/ffgc.2020.507710.
Gwenzi, D., Lefsky, M.A., Suchdeo, V.P., Harding, D.J., 2016. Prospects of the ICESat-2 laser altimetry mission for savanna ecosystem structural studies based on airborne simulation data. ISPRS J. Photogramm. Remote Sens. 118, 68–82. https://doi.org/10.1016/j.isprsjprs.2016.04.009.
Hall, F.G., Bergen, K., Blair, J.B., Dubayah, R., Houghton, R., Hurtt, G., Wickland, D., 2011. Characterizing 3D vegetation structure from space: Mission requirements. Remote Sens. Environ. 115 (11), 2753–2775.
Hancock, S., Armston, J., Hofton, M., Sun, X., Tang, H., Duncanson, L.I., Dubayah, R., 2019. The GEDI simulator: A large-footprint waveform lidar simulator for calibration and validation of spaceborne missions. Earth Space Sci. 6 (2), 294–310. https://doi.org/10.1029/2018EA000506.
Hantson, S., Pueyo, S., Chuvieco, E., 2015. Global fire size distribution is driven by human impact and climate. Glob. Ecol. Biogeogr. 24 (1), 77–86. https://doi.org/10.1111/geb.12246.
Harding, D.J., Carabajal, C.C., 2005. ICESat waveform measurements of within-footprint topographic relief and vegetation vertical structure. Geophys. Res. Lett. 32 (21), 4. https://doi.org/10.1029/2005GL023471.
Healey, S.P., Yang, Z., Gorelick, N., Ilyushchenko, S., 2020. Highly local model calibration with a new GEDI LiDAR asset on Google earth engine reduces Landsat Forest height signal saturation. Remote Sens. 12 (17), 2840. https://doi.org/10.3390/rs12172840.
Hermosilla, T., Coops, N.C., Ruiz, L.A., Moskal, L.M., 2014. Deriving pseudo-vertical waveforms from small-footprint full-waveform LiDAR data. Remote Sens. Lett. 5 (4), 332–341. https://doi.org/10.1080/2150704X.2014.903350.
Hoffmann, W.A., Jaconis, S.Y., McKinley, K.L., Geiger, E.L., Gotsch, S.G., Franco, A.C., 2012. Fuels or microclimate? Understanding the drivers of fire feedbacks at

savanna–forest boundaries. Aust. Ecol. 37 (6), 634–643. https://doi.org/10.1111/j.1442-9993.2011.02324.x.
Hofton, M., Blair, J.B., 2019. Algorithm Theoretical Basis Document (ATBD) for GEDI Transmit and Receive Waveform Processing for L1 and L2 Products. https://lpdaac.usgs.gov/documents/581/GEDI_WF_ATBD_v1.0.pdf. (Accessed 13 March 2021).
Hu, T., Ma, Q., Su, Y., Battles, J.J., Collins, B.M., Stephens, S.L., Kelly, M., Guo, Q., 2019. A simple and integrated approach for fire severity assessment using bi-temporal airborne LiDAR data. Int. J. Appl. Earth Obs. Geoinf. 78, 25–38. https://doi.org/10.1016/j.jag.2019.01.007.
Hudak, A.T., Bright, B.C., Pokswinski, S.M., Loudermilk, E.L., O'Brien, J.J., Hornsby, B. S., Silva, C.A., 2016a. Mapping forest structure and composition from low-density LiDAR for informed forest, fuel, and fire management at Eglin air Force Base, Florida, USA. Can. J. Remote. Sens. 42 (5), 411–427. https://doi.org/10.1080/07038992.2016.1217482.
Hudak, A.T., Dickinson, M.B., Bright, B.C., Kremens, R.L., Loudermilk, E.L., O'Brien, J.J., Ottmar, R.D., 2016b. Measurements relating fire radiative energy density and surface fuel consumption–RxCADRE 2011 and 2012. Int. J. Wildland Fire 25 (1), 25–37. https://doi.org/10.1080/07038992.2016.1217482.
Jakubowksi, M.K., Guo, K., Collins, B., Stephens, S., Kelly, M., 2013. Predicting surface fuel models and fuel metrics using Lidar and CIR imagery in a dense, mountainous forest. Photogramm. Eng. Remote Sens. 79 (1), 37–49. https://doi.org/10.14358/PERS.79.1.37.
Keane, R.E., Reeves, M., 2012. Use of expert knowledge to develop fuel maps for wildland fire management. In: Perera, A.H., et al. (Eds.), Expert Knowledge and Its Application in Landscape Ecology. Springer, pp. 211–228. https://doi.org/10.1007/978-1-4614-1034-8_11.
Keane, R.E., Herynk, J.M., Toney, C., Urbanski, S.P., Lutes, D.C., Ottmar, R.D., 2013. Evaluating the performance and mapping of three fuel classification systems using Forest inventory and analysis surface fuel measurements. For. Ecol. Manag. 305, 248–263. https://doi.org/10.1016/j.foreco.2013.06.001.
Kimura, T., Imai, T., Sakaizawa, D., Murooka, J., Mitsuhashi, R., 2017. The overview and status of vegetation Lidar mission, MOLI. In: 2017 IEEE International Geoscience and Remote Sensing Symposium (IGARSS). IEEE, pp. 4228–4230. https://doi.org/10.1109/IGARSS.2017.8127935.
Klauberg, C., Hudak, A.T., Silva, C.A., Lewis, S.A., Robichaud, P.R., Jain, T.B., 2019. Characterizing fire effects on conifers at tree level from airborne laser scanning and high-resolution, multispectral satellite data. Ecol. Model. 412, 108820. https://doi.org/10.1016/j.ecolmodel.2019.108820.
Kuhn, M., Wing, J., Weston, S., Williams, A., Keefer, C., Engelhardt, A., Benesty, M., 2020. Package 'caret'. R Journal 223.
Lang, N., Schindler, K., Wegner, J.D., 2019. Country-wide high-resolution vegetation height mapping with Sentinel-2. Remote Sens. Environ. 233, 111347. https://doi.org/10.1016/j.rse.2019.111347.
Lê, S., Josse, J., Husson, F., 2008. FactoMineR: an R package for multivariate analysis. J. Stat. Softw. 25 (1), 1–18.
Lefsky, M.A., Harding, D.J., Keller, M., Cohen, W.B., Carabajal, C.C., Espirito-Santo, F.D., 2005. Estimates of forest canopy height and aboveground biomass using ICESat. Geophys. Res. Lett. 32 (22) https://doi.org/10.1029/2005GL023971.
Lefsky, M.A., Harding, D.J., Keller, M., Cohen, W.B., Carabajal, C.C., Espirito-Santo, F.D., de Camargo, P.B., 2006. Correction to "estimates of forest canopy height and aboveground biomass using ICESat". Geophys. Res. Lett. 32 (5), L05501 https://doi.org/10.1029/2005GL025518.
Lefsky, M.A., Keller, M., Pang, Y., De Camargo, P.B., Hunter, M.O., 2007. Revised method for forest canopy height estimation from geoscience laser altimeter system waveforms. J. Appl. Remote. Sens. 1 (1), 013537 https://doi.org/10.1117/1.2795724.
Lehmann, C.E.R., Anderson, T.M., Sankaran, M., Higgins, S.I., Archibald, S., Hoffmann, W.A., Hanan, N.P., Williams, R.J., Fensham, R.J., Felfili, J., Hutley, L.B., Ratnam, J., San Jose, J., Montes, R., Franklin, D., Russell-Smith, J., Ryan, C.M., Durigan, G., Hiernaux, P., Haidar, R., Bowman, D.M.J.S., Bond, W.J., 2014. Savanna vegetation-fire-climate relationships differ among continents. Science 343, 548–552. https://doi.org/10.1126/science.1247355.
Li, W., Niu, Z., Shang, R., Qin, Y., Wang, L., Chen, H., 2020. High-resolution mapping of Forest canopy height using machine learning by coupling ICESat-2 LiDAR with Sentinel-1, Sentinel-2 and Landsat-8 data. Int. J. Appl. Earth Obs. Geoinf. 92, 102163. https://doi.org/10.1016/j.jag.2020.102163.
MacArthur, R.H., Horn, H.S., 1969. Foliage profile by vertical measurements. Ecology 50 (5), 802–804. https://doi.org/10.2307/1933693.
Marselis, S.M., Tang, H., Armston, J.D., Calders, K., Labrière, N., Dubayah, R., 2018. Distinguishing vegetation types with airborne waveform lidar data in a tropical forest-savanna mosaic: A case study in Lopé National Park, Gabon. Remote Sens. Environ. 216, 626–634.
Marselis, S.M., Tang, H., Armston, J., Abernethy, K., Alonso, A., Barbier, N., Dubayah, R., 2019. Exploring the relation between remotely sensed vertical canopy structure and tree species diversity in Gabon. Environ. Res. Lett. 14 (9), 094013.
Marshak, C., Simard, M., Duncanson, L., Silva, C.A., Denbina, M., Liao, T.H., Armston, J., 2020. Regional tropical aboveground biomass mapping with L-band repeat-pass interferometric radar, sparse Lidar, and multiscale Superpixels. Remote Sens. 12 (12), 2048. https://doi.org/10.3390/rs12122048.
Mauro, F., Hudak, A.T., Fekety, P.A., Frank, B., Temesgen, H., Bell, D.M., McCarley, T.R., 2021. Regional modeling of Forest fuels and structural attributes using airborne laser scanning data in Oregon. Remote Sens. 13 (2), 261. https://doi.org/10.3390/rs13020261.
Murooka, J., Kobayashi, T., Imai, T., Suzuki, K., Sakaizawa, D., Yamakawa, S., Asai, K., 2013. Overview of Japan's spaceborne vegetation lidar mission. In: Lidar Technologies, Techniques, and Measurements for Atmospheric Remote Sensing IX, vol. 8894. International Society for Optics and Photonics, p. 88940B.
Myers, N., Mittermeier, R.A., Mittermeier, C.G., Da Fonseca, G.A., Kent, J., 2000. Biodiversity hotspots for conservation priorities. Nature 403 (6772), 853–858. https://doi.org/10.1117/12.2029119.
Narine, L.L., Popescu, S., Neuenschwander, A., Zhou, T., Srinivasan, S., Harbeck, K., 2019. Estimating aboveground biomass and forest canopy cover with simulated ICESat-2 data. Remote Sens. Environ. 224, 1–11. https://doi.org/10.1016/j.rse.2019.01.037.
Narine, L.L., Popescu, S.C., Malambo, L., 2020. Using ICESat-2 to estimate and map forest aboveground biomass: A first example. Remote Sens. 12 (11), 1824.
Ogle, S.M., Kurz, W.A., Green, C., Brandon, A., Baldock, J., Domke, G., Herold, M., Bernoux, M., Waterworth, R.M., 2019. Chapter 2: Generic methodologies applicable to multiple land-use categories. In: 2019 Refinement to the 2006 IPCC Guidelines for National Greenhouse Gas Inventories, pp. 1–59.
Oliveira, U., Soares-Filho, B., de Souza Costa, W.L., Gomes, L., Bustamante, M., Miranda, H., 2021. Modeling fuel loads dynamics and fire spread probability in the Brazilian Cerrado. For. Ecol. Manag. 482 https://doi.org/10.1016/j.foreco.2020.118889.
Pardini, M., Armston, J., Qi, W., Lee, S.K., Tello, M., Bes, V.C., Fatoyinbo, L.E., 2019. Early lessons on combining lidar and multi-baseline SAR measurements for forest structure characterization. Surv. Geophys. 40 (4), 803–837. https://doi.org/10.1007/s10712-019-09553-9.
Patterson, P.L., Healey, S.P., Ståhl, G., Saarela, S., Holm, S., Andersen, H.E., Yang, Z., 2019. Statistical properties of hybrid estimators proposed for GEDI—NASA's global ecosystem dynamics investigation. Environ. Res. Lett. 14 (6), 065007 https://doi.org/10.1088/1748-9326/ab18df.
Pesonen, A., Maltamo, M., Eerikäinen, K., Packalèn, P., 2008. Airborne laser scanning-based prediction of coarse woody debris volumes in a conservation area. For. Ecol. Manag. 255 (8–9), 3288–3296. https://doi.org/10.1016/j.foreco.2008.02.017.
Peterson, B., Nelson, K., Wylie, B., 2013. Towards integration of GLAS into a national fuel mapping program. Photogramm. Eng. Remote Sens. 79 (2), 175–183. https://doi.org/10.14358/PERS.79.2.175.
Popescu, S.C., Zhao, K., Neuenschwander, A., Lin, C., 2011. Satellite lidar vs. small footprint airborne lidar: comparing the accuracy of aboveground biomass estimates and forest structure metrics at footprint level. Remote Sens. Environ. 115 (11), 2786–2797. https://doi.org/10.1016/j.rse.2011.01.026.
Popescu, S.C., Zhou, T., Nelson, R., Neuenschwander, A., Sheridan, R., Narine, L., Walsh, K.M., 2018. Photon counting LiDAR: an adaptive ground and canopy height retrieval algorithm for ICESat-2 data. Remote Sens. Environ. 208, 154–170. https://doi.org/10.1016/j.rse.2018.02.019.
Potapov, P., Li, X., Hernandez-Serna, A., Tyukavina, A., Hansen, M.C., Kommareddy, A., Hofton, M., 2021. Mapping global forest canopy height through integration of GEDI and Landsat data. Remote Sens. Environ. 253, 112165. https://doi.org/10.1016/j.rse.2020.1121.
Price, O.F., Gordon, C.E., 2016. The potential for LiDAR technology to map fire fuel hazard over large areas of Australian forest. J. Environ. Manag. 181, 663–673. https://doi.org/10.1016/j.jenvman.2016.08.042.
Qi, W., Dubayah, R.O., 2016. Combining Tandem-X InSAR and simulated GEDI lidar observations for forest structure mapping. Remote Sens. Environ. 187, 253–266. https://doi.org/10.1016/j.rse.2016.10.018.
Qi, W., Lee, S.K., Hancock, S., Luthcke, S., Tang, H., Armston, J., Dubayah, R., 2019. Improved forest height estimation by fusion of simulated GEDI Lidar data and TanDEM-X InSAR data. Remote Sens. Environ. 221, 621–634. https://doi.org/10.1016/j.rse.2018.11.035.
Quegan, S., Le Toan, T., Chave, J., Dall, J., Exbrayat, J.F., Minh, D.H.T., Williams, M., 2019. The European Space Agency BIOMASS mission: measuring forest above-ground biomass from space. Remote Sens. Environ. 227, 44–60. https://doi.org/10.1016/j.rse.2019.03.032.
R Core Team, 2020. R: A Language and Environment for Statistical Computing. R Foundation for Statistical Computing, Vienna, Austria. https://www.R-project.org/. (Accessed 13 March 2021).
Rishmawi, K., Huang, C., Zhan, X., 2021. Monitoring key Forest structure attributes across the conterminous United States by integrating GEDI LiDAR measurements and VIIRS data. Remote Sens. 13 (3), 442. https://doi.org/10.3390/rs13030442.
Roberts, D.A., Dennison, P.E., Gardner, M.E., Hetzel, Y., Ustin, S.L., Lee, C.T., 2003. Evaluation of the potential of Hyperion for fire danger assessment by comparison to the airborne visible/infrared imaging spectrometer. IEEE Trans. Geosci. Remote Sens. 41, 1297–1310. https://doi.org/10.1109/TGRS.2003.812904.
Roitman, I., Bustamante, M.M.C., Haidar, R.F., Shimbo, J.Z., Abdala, G.C., Eiten, G., Fagg, C.W., Felfili, M.C., Felfili, J.M., Jacobson, T.K.B., Lindoso, G.S., Keller, M., Lenza, E., Miranda, S.C., Pinto, J.R.R., Rodrigues, A.A., Delitti, W.B.C., Roitman, P., Sampaio, J.M., 2018. Optimizing biomass estimates of savanna woodland at different spatial scales in the Brazilian Cerrado: re-evaluating allometric equations and environmental influences. PLoS One 13, 1–21. https://doi.org/10.1371/journal.pone.0196742.
Rosan, T.M., Aragão, L.E., Oliveras, I., Phillips, O.L., Malhi, Y., Gloor, E., Wagner, F.H., 2019. Extensive 21st-century woody encroachment in South America's savanna. Geophys. Res. Lett. 46 (12), 6594–6603.
Rosen, P.A., Hensley, S., Shaffer, S., Veilleux, L., Chakraborty, M., Misra, T., Satish, R., 2015, May. The NASA-ISRO SAR mission-An international space partnership for science and societal benefit. In: 2015 IEEE Radar Conference (RadarCon). IEEE, pp. 1610–1613.
Saarela, S., Holm, S., Healey, S.P., Andersen, H.E., Petersson, H., Prentius, W., Ståhl, G., 2018. Generalized hierarchical model-based estimation for aboveground biomass

assessment using GEDI and Landsat data. Remote Sens. 10 (11), 1832. https://doi.org/10.3390/rs10111832.
Saatchi, S., Halligan, K., Despain, D.G., Crabtree, R.L., 2007. Estimation of forest fuel load from radar remote sensing. IEEE Trans. Geosci. Remote Sens. 45 (6), 1726–1740. https://doi.org/10.1109/TGRS.2006.887002.
Sanchez-Lopez, N., Boschetti, L., Hudak, A.T., Hancock, S., Duncanson, L.I., 2020. Estimating time since the last stand-replacing disturbance (TSD) from Spaceborne simulated GEDI data: A feasibility study. Remote Sens. 12 (21), 3506. https://doi.org/10.3390/rs12213506.
Sandberg, D.V., Ottmar, R.D., Cushon, G.H., 2001. Characterizing fuels in the 21st century. Int. J. Wildland Fire 10 (4), 381–387. https://doi.org/10.1071/WF01036.
Schmidt, I.B., Moura, L.C., Ferreira, M.C., Eloy, L., Sampaio, A.B., Dias, P.A., Berlinck, C. N., 2018. Fire management in the Brazilian savanna: first steps and the way forward. J. Appl. Ecol. 55 (5), 2094–2101. https://doi.org/10.1111/1365-2664.13118.
Schneider, F.D., Ferraz, A., Hancock, S., Duncanson, L.I., Dubayah, R.O., Pavlick, R.P., Schimel, D.S., 2020. Towards mapping the diversity of canopy structure from space with GEDI. Environ. Res. Lett. 15 (11), 115006. https://doi.org/10.5068/D16T06.
Silva, C.A., Saatchi, S., Garcia, M., Labriere, N., Klauberg, C., Ferraz, A., Hudak, A.T., 2018. Comparison of small-and large-footprint lidar characterization of tropical forest aboveground structure and biomass: a case study from Central Gabon. IEEE J. Sel. Top. Appl. Earth Observ. Remote Sens. 11 (10), 3512–3526. https://doi.org/10.1109/JSTARS.2018.2816962.
Silva, C.A., Hamamura, C., Valbuena, R., Hancock, S., Cardil, A., Broadbent, E.N., Almeida, D.R.A., Silva Junior, C.H.L., Klauberg, C., 2020. rGEDI: NASA's Global Ecosystem Dynamics Investigation (GEDI) Data Visualization and Processing. Version 0.1.8, accessed on October. 22 2020, available at. https://CRAN.R-project.org/package=rGEDI.
Silva, C.A., Duncanson, L., Hancock, S., Neuenschwander, A., Thomas, N., Hofton, M., Fatoyinbo, L., Simard, M., Marshak, C.Z., Armston, J., Lutchke, S., Dubayah, R., 2021. Fusing simulated GEDI, ICESat-2 and NISAR data for regional aboveground biomass mapping. Remote Sens. Environ. 253. https://doi.org/10.1016/j.rse.2020.112234.
Simon, M.F., Grether, R., Queiroz, L.P., Skema, C., Pennington, R.T., Hughes, C.E., 2009. Recent assembly of the Cerrado, a Neotropical plant diversity hotspot, by in situ evolution of adaptations to fire. Proc. Natl. Acad. Sci. USA 106 (48), 20359–20364. https://doi.org/10.1073/pnas.0903410106.
Souza, C.M., Shimbo, J.Z., Rosa, M.R., Parente, L.L., Alencar, A.A., Rudorff, B.F.T., Hasenack, H., Matsumoto, M., Ferreira, L.G., Souza-Filho, P.W.M., de Oliveira, S.W., Rocha, W.F., Fonseca, A.V., Marques, C.B., Diniz, C.G., Costa, D., Monteiro, D., Rosa, E.R., Vélez-Martin, E., Weber, E.J., Lenti, F.E.B., Paternost, F.F., Pareyn, F.G. C., Siqueira, J.V., Viera, J.L., Neto, L.C.F., Saraiva, M.M., Sales, M.H., Salgado, M.P. G., Vasconcelos, R., Galano, S., Mesquita, V.V., Azevedo, T., 2020. Reconstructing three decades of land use and land cover changes in brazilian biomes with landsat archive and earth engine. Remote Sens. 12 https://doi.org/10.3390/RS12172735.
Stavros, E.N., Coen, J., Peterson, B., Singh, H., Kennedy, K., Ramirez, C., Schimel, D., 2018. Use of imaging spectroscopy and LIDAR to characterize fuels for fire behavior prediction. Remote Sens. Appl. 11, 41–50. https://doi.org/10.1016/j.rsase.2018.04.010.
Stefanidou, A., Gitas, I.Z., Korhonen, L., Stavrakoudis, D., Georgopoulos, N., 2020. LiDAR-based estimates of canopy base height for a dense uneven-aged structured forest. Remote Sens. 12 (10), 1565. https://doi.org/10.3390/rs12101565.
Strassburg, B.B., Brooks, T., Feltran-Barbieri, R., Iribarrem, A., Crouzeilles, R., Loyola, R., Balmford, A., 2017. Moment of truth for the Cerrado hotspot. Nat. Ecol. Evol. 1 (4), 1–3. https://doi.org/10.1038/s41559-017-0099.
Szpakowski, D.M., Jensen, J.L., 2019. A review of the applications of remote sensing in fire ecology. Remote Sens. 11 (22), 2638. https://doi.org/10.3390/rs11222638.
Tang, H., Armston, J., 2019. Algorithm Theoretical Basis Document (ATBD) for GEDI L2B Footprint Canopy Cover and Vertical Profile Metrics. https://lpdaac.usgs.gov/documents/588/GEDI_FCCVPM_ATBD_v1.0.pdf. (Accessed 13 March 2021).
Turner, M.G., Gardner, R.H., O'neill, R.V., 1995. Ecological dynamics at broad scales. BioScience 45, S29–S35.
Wulder, M.A., White, J.C., Nelson, R.F., Næsset, E., Ørka, H.O., Coops, N.C., Hilker, T., Bater, C.W., Gobakken, T., 2012. Lidar sampling for large-area forest characterization: A review. Remote Sens. Environ. 121, 196–209. https://doi.org/10.1016/j.rse.2012.02.001.
Xiao, J., Chevallier, F., Gomez, C., Guanter, L., Hicke, J.A., Huete, A.R., Ichii, K., Ni, W., Pang, Y., Rahman, A.F., Sun, G., Yuan, W., Zhang, L., Zhang, X., 2019. Remote sensing of the terrestrial carbon cycle: A review of advances over 50 years. Remote Sens. Environ. 233, 111383. https://doi.org/10.1016/j.rse.2019.111383.
Yang, W., Ni-Meister, W., Lee, S., 2011. Assessment of the impacts of surface topography, off-nadir pointing and vegetation structure on vegetation lidar waveforms using an extended geometric optical and radiative transfer model. Remote Sens. Environ. 115 (11), 2810–2822. https://doi.org/10.1016/j.rse.2010.02.021.
Zanne, A., Lopez-Gonzalez, G., Coomes, D., Ilic, J., Jansen, S., Lewis, S., Miller, R., Swenson, N., Wiemann, M., Chave, J., 2009. Data from: towards a worldwide wood economics spectrum. Dryad Digital Reposit. https://doi.org/10.5061/dryad.234.
Zwally, H.J., Schutz, B., Abdalati, W., Abshire, J., Bentley, C., Brenner, A., Thomas, R., 2002. ICESat's laser measurements of polar ice, atmosphere, ocean, and land. J. Geodyn. 34 (3–4), 405–445. https://doi.org/10.1016/S0264-3707(02)00042-X.